Plug-in On-Board Single-Phase Cuk-Derived Bridgeless EV Charger for AC and DC Charging Systems

Sukanya Dutta

A Thesis

In the Department

of

Electrical and Computer Engineering

Presented in Partial Fulfillment of the Requirements

For the Degree of Master of Applied Science (Electrical and Computer Engineering) at

Concordia University

Montreal, Quebec, Canada.

August 2021

CONCORDIA UNIVERSITY
SCHOOL OF GRADUATE STUDIES

This is to certify that the thesis prepared

By: Sukanya Dutta

Entitled: Plug-in On-Board Single-Phase Cuk-Derived Bridgeless EV Charger for AC and DC Charging Systems

and submitted in partial fulfillment of the requirements for the degree of

Master of Applied Science (Electrical and Computer Engineering)

Complies with the regulations of this University and meets the accepted standards with respect to originality and quality.

Signed by the final examining committee:

_____ Chair
Dr. Chunyan Lai

_____ Examiner, External
Dr. Anjali Awasthi To the Program

_____ Examiner
Dr. Chunyan Lai

_____ Supervisor
Dr. Akshay Kumar Rathore

Approved by: _____
Dr. Yousef R. Shayan, Chair
Department of Electrical and Computer Engineering

August 5th, 2021
Date of Defence

_____
Dr. Mourad Debbabi, Interim Dean
Gina Cody School of Engineering and Computer Science

ABSTRACT

Plug-in On-Board Single-Phase Cuk-Derived Bridgeless EV Charger for AC and DC Charging Systems

Sukanya Dutta, M.A.Sc.
Concordia University, 2021

Electric vehicles (EVs) have recently garnered popularity in the consumer market due to its environment friendly nature as it uses clean energy to power vehicles. The EVs that are on road majorly comprise of two-wheeler, E-rickshaw, intralogistics equipment, trio, golf carts, short range mobility vehicle, which come under the category of low power EVs and passenger buses, loading trucks, electric trucks, which fall under the category of high power EVs. Batteries are the primary source of energy to power these EVs. Therefore, to recharge these batteries a battery charger is required. The conventional battery chargers have the merit of easy implementation but have higher component count, lower efficiency, complex control, low input power quality, and inflexible charging options. In order to achieve unity power factor (UPF), low THD, and high power quality; a power factor correction (PFC) unit becomes a crucial part of the AC-DC converters of the battery charger. The DCM design proves advantageous due to its inherent PFC operation at the input side, reduction of switching losses due to zero turn-on losses as well as zero reverse recovery diode losses. Also, the control circuit becomes simple as it requires only a single control loop and a single sensor. Thereby, making the converter reliable and robust towards high frequency noise. Further, to make the EV battery chargers flexible and to combat range anxiety, vehicle-to-vehicle power transfer aids in solving the issue.

This thesis analyses and designs a single-phase bridgeless Cuk-derived converter as on-board EV charger for AC and DC charging systems. At first, a single sensor based Cuk-derived PFC AC-DC converter has been analyzed and studied which has the advantages of lower component count, improved efficiency, high power quality, and low cost. The converter is designed in DCM to accomplish PFC naturally on the input side. The voltage stress is lower compared to the conventional Cuk converter thereby, reducing the switching losses and enhancing the overall system efficiency. The converter control is simple requiring only one

voltage loop and sensor. The detailed small-signal modelling using the current injected equivalent circuit approach and controller design has been presented. Further, to enhance the charging flexibility to mitigate the range anxiety, the same topology has been analyzed and designed for V2V charge transfer. A novel charge transfer technique has been implemented using the same topology. The loss analysis for both configurations has been reported in detail. The steady-state analysis and converter design for both configurations has been provided. Simulation results from PSIM 11 as well as proof-of-concept hardware prototype results are discussed extensively to validate the converter analysis, design and high performance.

Acknowledgment

I would like to express my deepest gratitude and sincere appreciation to my supervisor, *Prof. Akshay Kumar Rathore* for his esteemed guidance, support, and patience throughout my Master studies. I would like to thank him for his thoughtful suggestions and assistance in my research, which has been fundamental in the completion of this thesis. I have learnt a lot from his scientific knowledge, simplicity, and punctuality, which are essential for any success. I would also like to convey my thanks to the committee members, *Prof. Chunyan Lai, Prof. Anjali Awasthi*, and *Prof. Akshay Kumar Rathore* for serving as my committee.

I would like to thank Concordia University for this opportunity, the world-class research facility, and financial support. I would like to thank all the staff and faculty members for their kindness and support.

I extend my gratitude towards *Dr. Sivanagaraju, Dr. Venkata, Dr. Mathews, Dr. Swati, Abhinandan,* and *Karan* for their suggestions and support in building the experimental setup as well as the fruitful technical discussions. Heartfelt thanks to my colleagues *Koyelia, Ronak, Gayathri, Mohanraj, Nil, Dwaipayan*, and all the members of PEER group for their friendship and moral support.

I would like to thank my parents and sister (*Mr. Biswabijoy Dutta, Mrs. Nina Dutta, and Ms. Sunanda Dutta*) for their unconditional love and support throughout my life. Also, I would like to express gratefulness towards all the members of my family.

In the end, I would like to acknowledge my friends for their generosity, support, and friendship throughout my thesis.

Table of Contents

List of Tables

List of Figures

List of Abbreviation

EVs	Electric Vehicles
ICE	Internal Combustion Engine
BEVs	Battery Electric Vehicles
HEVs	Hybrid Electric Vehicles
FCEVs	Fuel Cell Electric Vehicles
G2V	Grid-to-Vehicle
V2V	Vehicle-to-Vehicle
AEVs	All Electric Vehicles
V2G	Vehicle-to-Grid
V2H	Vehicle-to-Home
OBCs	On-board Battery Charger
BMS	Battery Management System
PFC	Power Factor Correction
THD	Total Harmonic Distortion
EMI	Electromagnetic Interference
CCM	Continuous Conduction Mode
DCM	Discontinuous Conduction Mode
AC	Alternating Current
DC	Direct Current
LC	Inductor-Capacitor
LLC	Inductor-Inductor-Capacitor
PI	Proportional Integral
RCD	Resistor-Capacitor-Diode

PSFB	Phase Shifted Full Bridge
ZVS	Zero Voltage Switching
UPF	Unity Power Factor
PWM	Pulse Width Modulation
MOSFET	Metal Oxide Semiconductor Field-Effect Transistor
RMS	Root Mean Square
PM	Phase Margin
PF	Power Factor
FFT	Fast Fourier Transform
INL	Idaho National Laboratory
A2A	AC-to-AC
D2D	DC-to-DC
D2A	DC-to-AC
A2D	AC-to-DC
A2B	AC-to-Battery
B2A	Battery-to-AC

List of Symbols

V_{in}	Input Voltage
V_o	Output Voltage
i_o	Output Current
D	Duty Cycle
L_{in}	Input Inductor
I_{Lin}	Input Inductor Current
V_{Lin}	Input Inductor Voltage
V_{Lo}	Output Inductor Voltage
V_{GS}	Gate Signal Voltage
i_{fw}	Freewheeling Current
L_o	Output Inductor
I_{Lo}	Output Inductor Current
L_{eq}	Equivalent Inductance
I_{Do1}, I_{Do2}	Output Diode Current
i_{sw}	Switch Current
V_{sw}	Switch Voltage
V_{Do1}, V_{Do2}	Output Diode Voltage
V_{Co1}, V_{Co2}	Output Capacitor Voltage
i_{Co1}, i_{Co2}	Output Capacitor Current
T_s	Switching Cycle Time Period
D_{o1}, D_{o2}	Output Diode
$I_{Do1,avg}$	Output Average Current
M	Converter Gain
M_{cr}	Critical Voltage Conversion Ratio
$V_{o,ripple}$	Output Voltage Ripple

$C_{O,}\ C_{O1,} C_{O2}$	Output Capacitors
C_t	Transfer Capacitor
V_{Ct}	Transfer Capacitor Voltage
i_{Ct}	Transfer Capacitor Current
f_s	Switching Frequency
$R_{\mathrm{o},} R_{\mathrm{out}}$	Load Resistance
$P_{o\mathrm{ut}}$	Converter Output Power
$V_{m,}\ V_{pk}$	Peak Input Voltage
I_{m}	Peak Input Current
f_{res}	Resonant Frequency
f_{in}	Input Frequency

CHAPTER 1: INTRODUCTION

1.1. Introduction

Owing to the reduced cost of vehicles, the demand for personal vehicle for transportation has grown significantly. Since internal combustion engine (ICE) vehicles have been relevant for over 100 years, the oil demand has significantly risen. The emission from these vehicles is a major reason for global warming [1]. Fig 1.1 represents the carbon dioxide emission of ICE vehicles in comparison to the electric vehicles (EVs) and Table 1.1 presents the commercial aspects of different vehicle types [2][3]. Thus, with the strict restrictions on emissions and fuel economy, the requirement of sustainable and eco-friendly sources of energy becomes essential and thereby, the alternative energy sources garnered immense attention in the past decades. One of the crucial needs to improve the environment condition is an alternative, clean, and efficient transportation system. EVs are a viable option to solve the energy crisis issue due to the transportation system. The recent advancement in the EVs technologies can be deemed as a constructive step towards clean automobile technology [4][5].

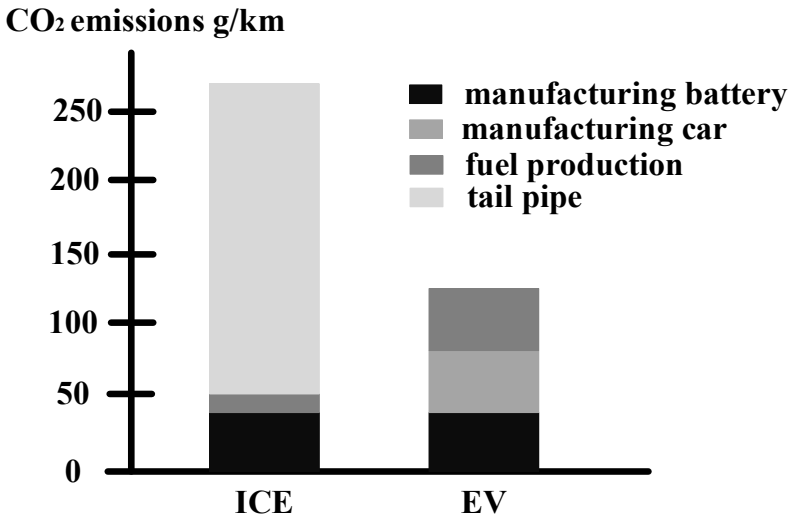

Fig 1.1. ICE vehicle V/S EV CO_2 emissions

The global EV sales have been rising rapidly and as per the analysis [6], by 2030 the global sales will increase to 120 million. The global fleet of plug-in light vehicles was 7.5 million by the end of 2019 [7]. The contribution of commercial medium and heavy plug-in vehicles to the global

Table 1.1: Commercial Aspects

Vehicle	Range	Refuel Time
Hydrogen Fuel Cell Vehicle	320-405km/200-250 miles	3-4 minutes
Electric Vehicle	160-500km/100-310 miles	30 minutes to 12 hours
Petrol or Diesel Vehicle	480-640km/300-400 miles	2-3 minutes

stock is 700,000 units [8]. The different types of EVs that are available in the market are the battery electric vehicles (BEVs), hybrid electric vehicle (HEVs), and fuel cell electric vehicles (FCEVs) as shown in Fig 1.2. These can be further majorly classified into two-wheelers, three-wheelers, and four-wheelers. Most of them require batteries as their energy source and to recharge these batteries the requirement of a battery charger becomes fundamental [9]. As the mass adoption of EVs are restrained because of the range anxiety, charging infrastructure requirement, and high cost. Increasing the battery capacity cannot be a feasible solution as it increases the weight and cost of the EVs. Therefore, the design of compact and cost-effective on-board battery charger enabling flexible charging techniques such as grid-to-vehicle (G2V) and vehicle-to-vehicle (V2V) without compromising the input current harmonic limitations as per standards [10] is crucial.

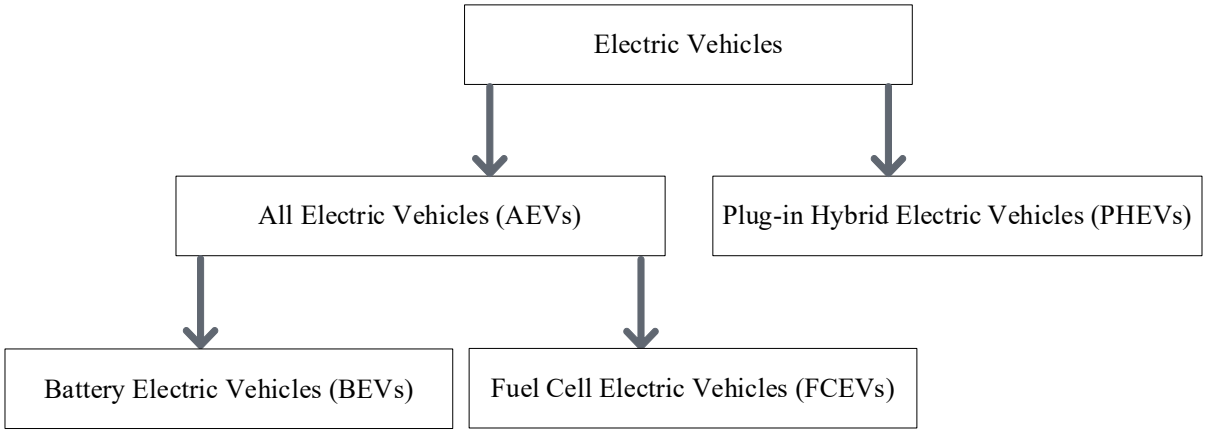

Fig 1.2. Types of electric vehicles

1.2. Classification of ALL Electric Vehicles

This section provides a description of the EVs namely BEVs and FCEVs which fall in the domain of all electric vehicles (AEVs) [4]. Table 1.2 lists the BEVs and FCEVs attributes.

1.2.1. Battery Electric Vehicles (BEVs)

BEVs are one of the solutions to combat the energy crisis and global warming issue. The electric motor drive based is the propulsion system of the BEVs. Battery and ultracapacitor are the energy storage systems in BEVs. Electric grid charging facilities and infrastructure are utilized to recharge the energy source. The basic characteristics of BEVs are zero emissions, high efficiency, independence from crude oils, and commercial availability. The disadvantages of BEVs are its high initial cost and range anxiety. To achieve the requisite driveability at the highest energy efficiency and the lowest emissions, the automotive engineering and electrical engineering have to come together for the optimal design. The main components of the BEVs are the motor, batteries, converter, controller, and energy management system.

Table 1.2: BEVs and FCEVs attributes

Attributes	**Battery Electric Vehicles (BEVs)**	**Fuel Cell Electric Vehicles (FCEVs)**
Propulsion System	Electric motor drives system	Electric Motor Drives System
Energy System	Batteries and ultracapacitors	Fuel cells, batteries, and ultracapacitors
Energy Source and Infrastructure	Electric grid based charging	Hydrogen
Basic Characteristics	Zero emission, highly energy efficient, free from crude oil, commercial availability	Ultra low emission, highly energy efficient, low crude oil dependence, sufficient driving range
Key Issues	Initial cost, range anxiety, battery and battery management, charging infrastructure	Under developed, high cost, reliability, cycle life, hydrogen infrastructure

The BEVs can transfer power in different modes such as grid-to-vehicle (G2V) where the EVs get charged from the grid, vehicle-to-vehicle (V2V) where the vehicle gets charged from another vehicle, vehicle-to-grid (V2G) where the power is transferred from the EV to the grid, vehicle-to-home (V2H)

where the power is transferred from the EV to home for emergency power backup. These features contributed to the solution of range anxiety issue thus, making the BEVs more commercially viable.

1.2.2. Fuel Cell Electric Vehicles (FCEVs)

FCEVs are emission free due to the fact that they utilize hydrogen for the production of electricity. The electricity thus produced is utilized for driving the vehicle or is preserved in the energy storage device such as batteries or ultracapacitors. The electricity produced here is through chemical reaction thus, there is no fuel burning and no pollutants production. Water and heat are the by-product of the fuel cells. The FCEVs operation is quiet. Similar to BEVs, the electric motor drive based is the propulsion system. The batteries or ultracapacitors are used at the starting for power density enhancement. The prime energy source is hydrogen in FCEVs. The important characteristics of FCEVs are ultra-low emission, high efficiency, low dependence on crude oil, and higher driving range. The disadvantages are high cost, safety, and hydrogen infrastructure. To ensure the efficiency, longevity, reliability, and optimum cost operation of FCEVs, the automotive engineering, electrical engineering, and fuel cell engineering integration are necessary to harness the gasoline and battery dependent new energy device. To achieve the requisite driving range at the highest efficiency and the lowest emission, the electric propulsion and fuel cell system must work very well together.

1.3. Category of EVs

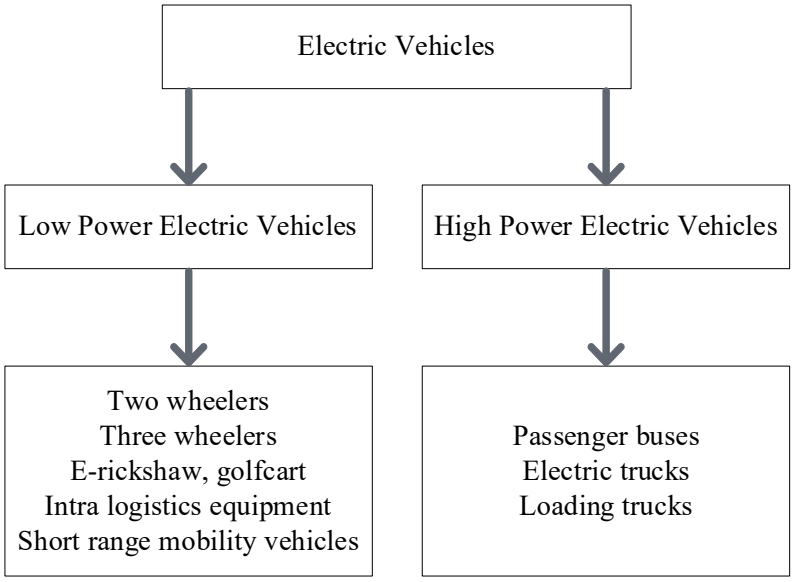

Fig 1.3. Categories of electric vehicles

The EVs can be divided into two categories based on battery voltage namely; (a) low power EVs having battery voltage 48V/72V and (b) high power EVs having battery voltage 400V/600V, which is shown in Fig. 1.3. Typical examples of low power EVs are two wheelers, three wheelers, golf carts, e-rickshaw, intra logistics equipment, short range mobility vehicles whereas passenger cars, electric buses are the examples of high power EVs. Table 1.3 lists the characteristics of different EV types [11].

Table 1.3: EV types with characteristics

Electric Vehicle	**Two-Wheeler/ E-rikshaw/ Intra Logistics Equipment**	**Trio/Golf Carts**	**Short Range Mobility Vehicle**	**Passenger cars/ Buses**
Battery Voltage	48V	48V	120V	400-600V
Charger Power	0.5-1kW	1-3kW	3.3-7kW	62-500kW
Charging time	6-8hrs	3-4hrs	4hrs	30mins

1.4. Electric Vehicle Battery Charging Infrastructure

This section describes the methods of battery charging such as the grid based AC charging, solar based DC charging and fast DC charging [12][13]. Different levels of EV charging are shown in Fig. 1.4 [14]. Fig 1.5 represents the basic AC charging and DC charging features [16].

Level 1	Supply from household outlet EV's onboard charger is used 120V 1ph AC; 12-16A
Level 2	Supply from household outlet or EV Charge point EV's onboard charger is used 208-240V 1ph AC; 12-80A (Typ. 30A)
Level 3	Supply from 208-600V 3ph AC Offboard DC fast charger is used 400A (Typ. 60A)

Fig 1.4. Different charging levels in North America

1.4.1. Grid based Slow AC Charging

This charging method uses low power and the usual charging time is 6-10 hours. This method is suitable for the EVs, which are charged during the night and driven in the daytime. The charging cost is low here as it uses the low night electricity price whereas the slow night charging can contribute to the increment of power grid load rate for the power grid companies during the night time. AC charging piles are utilized by on-board EV chargers in slow charging mode.

1.4.2. Medium Speed Charging

This method is to provide short time charging facilities for EVs and is based on 0.5C-1C charging current. 1-2 hours are required for full battery charging. The charging time is short and the charging current is less compared to the fast charging thus, the battery impacts are also less. This charging method is suitable for taxi drivers owing to its low charging time, which can be charged during lunch time/shift change and thereby, providing enough driving range for the next shift with less impact on the battery life. The size and investment of medium speed battery charger are lower compared to fast charging. If the power is less than 30kW, there is no requirement to construct the charging piles as a portable charger can be used in its place because any three-phase charging port can be utilized for the process. The construction of charging stations is not required; thereby reducing the investment. Also, the power grid effect is less.

1.4.3. Fast DC Charging

The fast DC charging current requirement is high which is about 1C-3C. It is usually used for emergency charging in particular on highways; It is a solution to the issue of short driving range and intercity drive but the disadvantage of this method is the battery lifetime impact as the current is high. Also, the requirement and considerations to develop a charging infrastructure are very high.

1.4.4. Solar based DC Charging

PV-grid and PV-standalone are two approaches to charge the EVs using PV. PV-grid charging can be conducted utilizing the grid during inadequate solar irradiance, which is an advantage. Also, the power can be injected into the grid in absence of EV. PV-standalone systems

are more suitable for remote areas where the utility supply is unavailable or costly. This system has simpler configuration due to the requirement of less power conversion stages. The grid stability is improved due to the availability of PV power.

1.4.5. Battery Swapping

In this method, batteries are replaced instead of charging the batteries. It takes only 5-10 minutes and is the fastest among all methods. But this method is based on several conditions such as standardisation of EV batteries as well as huge investment from the Government and power grids. The conditions are in fact difficult to implement. Further, professionals and expensive mechanical equipment are necessary for battery pack replacement. Lowest process time and the easy maintenance are the advantages of this method. But more space is needed to store more batteries and larger power lines are required for their charging power. Therefore, the initial investment is very high for such charging stations.

AC Charging	• EV charging at different speed • Alternating current or alternating power • Availability in power grid • Economic transmission over long distances • Converted to DC using power electronic converter • Low cost • Found in parking lots • More prevalent
DC Charging	• Fast EV charging • Direct current or direct power • Constant • Stored in batteries • High cost • Found in highways • Less prevalent

Fig 1.5. AC charging and DC charging features

1.5. Battery Charging Strategies and Temperature Effect:

The different battery charging strategies have been briefly discussed in this section [81].

(i) Constant current constant voltage (CC-CV),

(ii) Multi-step constant current (MSCC),

(iii) Boost charging,

(iv) Pulse charging

CC-CV is the standard charging strategy because of its simplified nature and easy implementation. The charging profile is shown in fig. 1.6. It is a two-stage charging process. The high current rate during the CC period will decrease the charging time. MSCC is an alternative charging strategy that aids in charging time reduction, energy efficiency improvement, and prolonged cycle life. The boost charging strategy has high charging current in the initial stage and requires a charger with high power capability. Its BMS system requires an extra timer functionality. The pulse charging strategy requires a large energy buffer device for its pulse current. The pulse charging without the large energy buffer such as inner battery storage will have deleterious effect on the power quality of the grid, which is caused due to the intermittent power demand. The overall efficiency of the charger is impacted due to different charging strategies because the power electronic converters generally have limited range of operation with optimal efficiency. Thus, it is important to select a charging strategy that matches the operation of the converter within its optimal efficiency range.

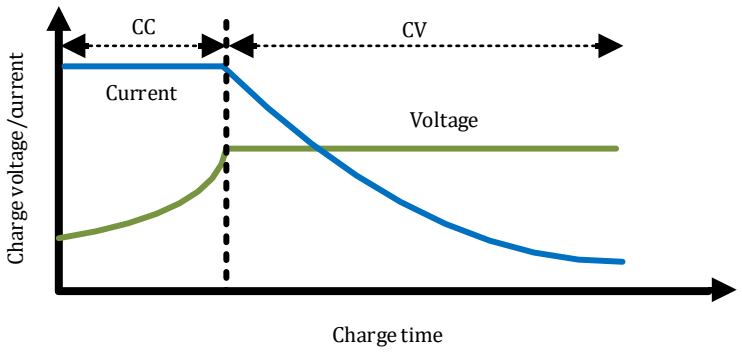

Fig 1.6. EV battery charging profile in CC-CV mode

The EV batteries can get degraded faster during hot climates as the rate and efficiency of chemical reactions occurring in the batteries are affected due to the high temperature [82][83]. High

temperature promotes faster reaction. Some chemical reactions that degrade the batteries occur faster at higher temperatures. Further, using a DC fast charger at such temperature can make the battery degrade at a higher rate as fast charging increases the temperature due to high electric current injection, which doubles the effect that hot weather has on the EV battery. In such cases, low power slow chargers can promote sustained battery health.

1.6. Thesis Objectives

The prime objective of the thesis is the investigation and implementation of G2V and V2V charging techniques using a single-phase universal converter. The advantages of the universal converter in comparison to the existing ones are the reduced components' count, simple control strategy with low sensor count along with PFC operation and low total harmonic distortion (THD). The AC-DC and DC-DC modes of operation are explored using the universal converter with primary goals to reduce components' count, improved power quality, flexible charging options to reduce range anxiety, and maintain overall efficiency. The converter is designed to operate in discontinuous conduction mode (DCM) to achieve natural PFC and thereby, reduced control requirements and sensors' count, which increases converter robustness. The power converter design is tested under source and load perturbations.

The main objectives of the thesis are:

1. Flexible charging
2. Components reduction
3. Simple control design and implementation

To accomplish the above-mentioned objectives, the thesis investigates and implements two charging techniques using the same topology, a brief description of the same is provided in the thesis outline and the detailed description is provided in Chapter 3 and Chapter 4.

1.7. Thesis Outline

The major contributions of the thesis are outlined as follows:

In Chapter 3, a single-phase bridgeless Cuk-derived PFC converter with reduced components' count for on-board G2V charging application is proposed. The converter output inductor is designed to operate in DCM to attain PFC naturally at the AC side, and thereby reducing

the sensor requirement, the cost of operation, and enhancing the converter robustness. The proposed bridgeless Cuk-derived converter has lower components' voltage stress, which results in decrement in the components' switching losses and efficiency enhancement. Throughout the converter operation range, only a single semiconductor device is in current flow path. Thus, reducing the converter losses due to conduction, and makes thermal management easy. The converter detailed steady-state analysis, converter design, small-signal-modeling, and closed loop controller design, and loss analysis are presented. The converter analysis and the design are validated with PSIM 11 simulation results as well as with a 1 kW proof-of-concept hardware prototype results.

In Chapter 4, a novel V2V charge transfer technique using the same bridgeless single phase Cuk-derived converter is proposed, studied and analysed in Chapter 3. The V2V charge transfer technique uses the on-board charger of only one EV, which reduces two redundant conversion stages and increases efficiency. Only dc-dc conversion and already available terminals are used to accomplish the charging process. The battery of one EV is charged using the battery of another EV. The detailed steady-state analysis, design in DC charging mode along with loss analysis and comparative study are reported. The validity of the proposed power converter in DC charging mode for the V2V power transfer is proved using PSIM 11 simulation results and a 500 W laboratory-based proof-of-concept hardware prototype.

1.8. Conclusion

This Chapter discussed the need to shift to EVs from conventional ICE vehicles owing to the strict emission restrictions and eco-friendly nature of the EVs. The commercial aspects of EVs, FCEVs, and ICE vehicles detailing the range and refuelling time are discussed. A brief description on classification and comparison of all electric vehicles (AEVs) namely battery electric vehicles (BEVs) and fuel cell electric vehicles (FCEVs) is presented. Categories of EVs along with their characteristics are outlined in this Chapter. Further, different EVs charging infrastructure such as grid based slow AC charging, medium speed charging, fast dc charging, solar based dc charging, and battery swapping are described.

Since, the battery charger system is a crucial part of electric vehicles, the next Chapter deals with a detailed review of state-of-art EV battery charger topologies for G2V charge transfer.

CHAPTER 2: ELECTRIC VEHICLE CHARGING SYSTEMS

2.1. Introduction

Battery packs are the power source for electric vehicles (EVs) and a battery charger is required to recharge these battery packs. A power electronic device converting AC voltage to required DC voltage and current level is known as a battery charger. EV battery chargers can be mainly classified into two types; namely a) Plug-in Chargers, and b) Wireless Chargers. Fig. 2.1 illustrates the types and sub-types of EV battery chargers. The wireless chargers can be further classified into inductive and capacitive. Inductive chargers are more efficient and have higher power rating whereas capacitive chargers are less efficient and have lower power ratings. Plug-in chargers are more popular comparatively because of the complicated design and low efficiency of the wireless chargers [15].

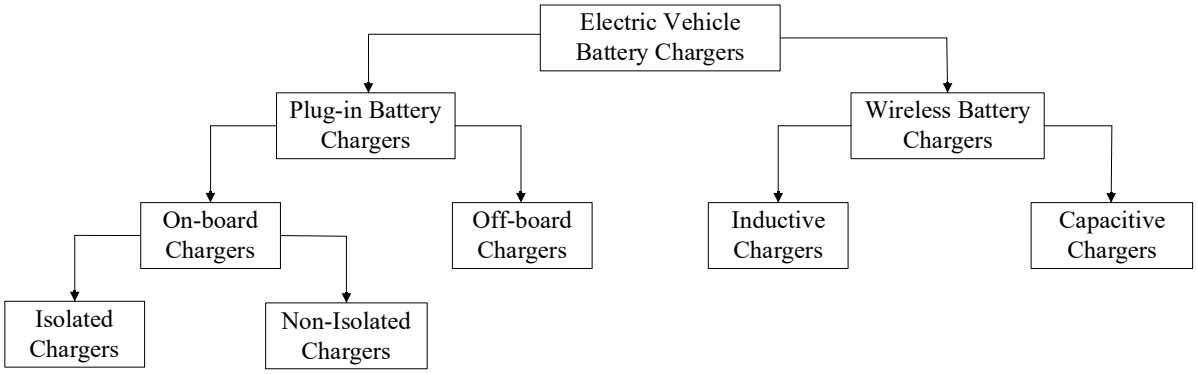

Fig 2.1. Electric Vehicle Battery Chargers Classification

2.2. Plug-in Battery Chargers

On-board and off-board chargers are the broad divisions of plug-in chargers. Table 2.1 lists the basic attributes of the on-board and the off-board battery chargers. Off-board chargers are capable of transferring higher kilowatts of power reducing battery charging time and has the requirement of exclusive power system for battery charging as well as advanced battery management systems (BMS). Off-board chargers are usually termed as fast chargers as an off-board charger of power rating more than 100 kW can charge the batteries within half an hour [11]. The off-board chargers aid in enhancing the overall efficiency of the vehicle as they are not placed

on the vehicle and thereby, reducing substantial weight from the EV. The major disadvantage of off-board chargers is the high current injection, which reflects in temperature rise and may require frequent battery maintenance and replacement. On the other hand, on-board chargers are slow chargers with lower power rating of about 3.3 kW or less, which are utilized by plugging-in to the AC mains. The on-board chargers can be classified into isolated and non-isolated chargers. The non-isolated topologies do not incorporate galvanic isolation since there is no electrical requirement of the battery to be isolated from the AC source [16]. Thus, the non-isolated topologies are compact, lightweight, and achieve higher efficiency [17]. The isolated chargers are heavier due to the inclusion of galvanic isolation, which is implemented using an high frequency transformer. The isolated chargers can be further divided into single-stage topologies and two stage topologies. These topologies as reported in literature have low efficiency owing to the leakage inductance and complicated control for the PFC acquirement [18] [19]. Based on the power level, these topologies charge the EV batteries within 4-7 hours. The current injection is low thus, the battery lifetime is enhanced as well as the maintenance is low. Two-stage non-isolated topologies incorporate higher number of switches and have higher losses [19].

Table 2.1: Attributes of Battery Charger

Type of Charger	Attributes
On-board Charger	• 120 VAC/ 240 VAC, 20 Amp/ 80 Amp, 1-phase • Low power transfer • Slow charger • Charging time – 4 to 12 hrs • On-board rectifier controls the BMS • Low battery heating • Weight addition
Off-board Charger	• 600 VDC/ 450 VAC, 400 Amp/ 200 Amp, 3- phase • High power transfer • Fast Charger • Charge within 30 minutes • Advanced BMS systems • Battery heating management • Zero weight added

2.3. Review of Conventional On-board Battery Charger Architectures

This Section provides a description of the conventional onboard battery chargers architectures reported in the literature for charging high voltage and low voltage EV battery packs. Advanced EVs employ high voltage lithium-ion based high voltage battery packs whereas low voltage lead-acid battery packs are deployed in two wheelers, e-rickshaw, golf carts, etc.

2.3.1. Single-Stage Isolated Structure

The single stage isolated structures are illustrated in Fig. 2.2 (a) and Fig. 2.2 (b) [20][21]. These structures comprise of diode bridge rectifier along with an isolated flyback converter/half-bridge DC-DC isolated resonant converter. Fig. 2.2 (a) is a common topology used for charging battery packs. It is a simple and effective battery charging solution. This charger has the advantage of lower components' count thereby, making it cost effective AC/DC PFC charger.

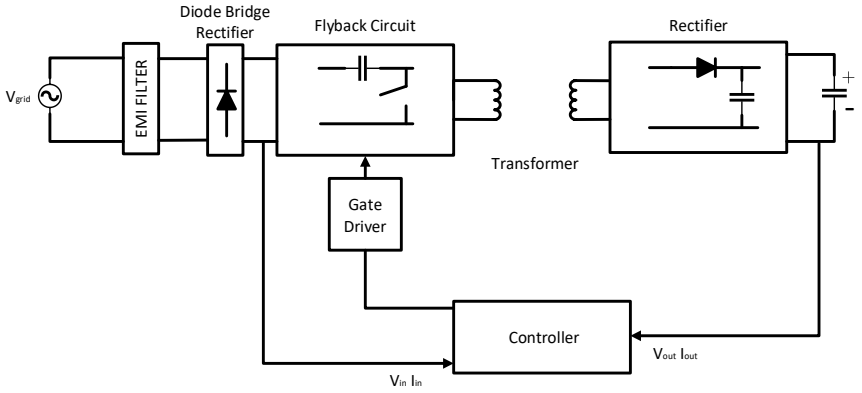

(a)

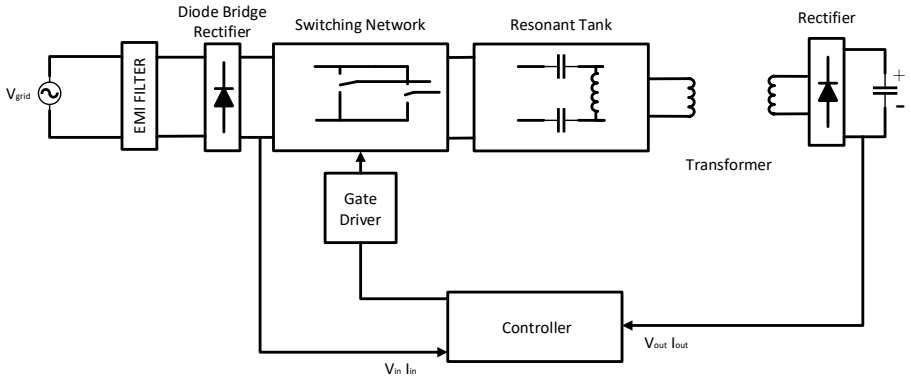

(b)

Fig 2.2. Single stage structures; (a) Isolated Flyback Converter; (b) Isolated Half Bridge DC-DC Resonant Converter;

Also, the control strategy for the converter is simpler. The major disadvantage of the isolated flyback converter topology is the effect of leakage inductance, which affects the switch voltage resulting in high voltage stress requiring overrated devices [21]. While turning off the switch, it has been observed that the discharge of leakage inductance of the transformer gives rise to a huge voltage spike across the switch. Therefore, for energy dissipation and to clamp the switch voltage, an external RCD snubber is connected, which results in additional losses [22]. Moreover, incorporation of diode on the secondary side involves hard switching operation leading to high power loss and thereby, reduction of converter efficiency. This topology is incapable of accomplishing PFC for various line voltages and provides low power factor and THD due to absence of active current wave shaping unit [20].

The half bridge series resonant converter as shown in Fig. 2.2 (b) is an improved topology for battery charger application. This topology undergoes soft switching because of the series resonant tank thus, the losses due to the leakage inductance are avoided. The development of this topology is basically based on the reduction of the switching losses. However, the topology incurs losses due to the presence of diode bridge rectifier which results in high conduction and turn on losses thereby, the thermal management requirements of the power converter become high [15]. Moreover, the PFC unit is not present in such battery charger topology, which reduces the power quality of the system. The LC filter present at the transformer secondary side induces duty cycle loss on the primary voltage of the transformer. Since the sudden change of current is restricted by the inductor, the diodes at the secondary are shorted resulting in duty cycle and rectifier snubber loss [16].

The battery charger configuration described above are float chargers [23]. These have easy control strategy with only a single control loop. These require current limiting resistors at the output and utilize single sensor making the battery charger less complicated. But these topologies require a diode bridge rectifier for AC to DC conversion which draws a peak input current. These configurations do not employ an active PFC unit at the front-end thereby, odd harmonics are injected into the grid that results into low power quality and high THD in grid current [24]. To filter out these harmonics, bulky filters are required, which increase the weight and volume of the charger.

2.3.2. Two-Stage Isolated Structure

Fig. 2.3 presents the two stage isolated configuration of a battery charger. These topologies garnered popularity in industries, which consist of a dedicated PFC unit and a battery charging control unit [25]. These chargers mainly are of two types; (a) Post-regulator type and (b) Pre-

regulator type. The post-regulator type as reported in [26] comprises of an isolated converter, which provides isolation from AC mains and a non-isolated converter for input current shaping and for battery charging process control. But these converters are less efficient due to high conduction losses in the primary side switches.

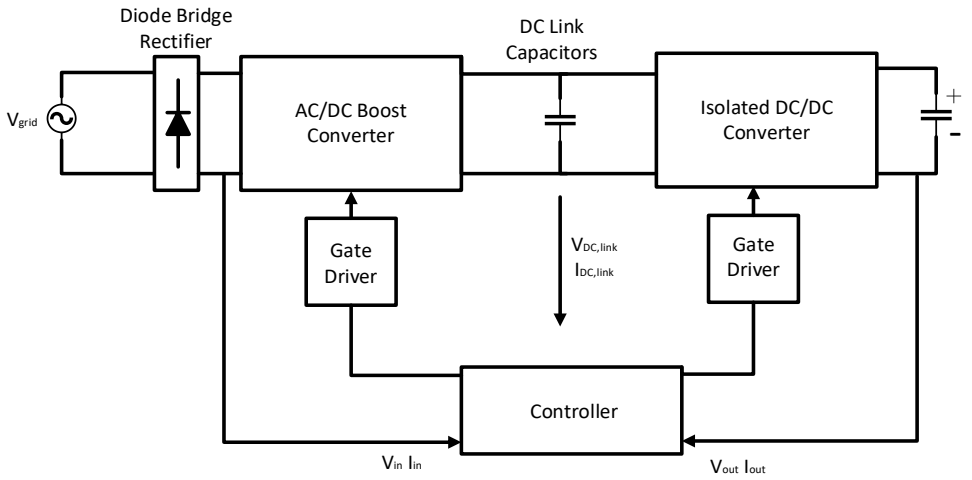

Fig 2.3. Two Stage Converter Configuration

Also, the current shaping unit has high losses due to conduction and switching losses therefore, this topology is not suitable for the charging of low voltage battery packs charging. However, a pre-regulator structure [27]-[29] has a non-isolated converter for the input current shaping for UPF operation and an isolated converter for the battery charging control. This topology is preferred in battery chargers for its higher reliability. The AC/DC PFC converter as the first stage consists of EMI filter, rectifier, PFC converter, and a DC link capacitor. The first stage converts the AC voltage to DC with PFC operation.

A high frequency signal controls the converter for input current shaping to accomplish UPF operation. The current shaping is done using one of the methods such as peak current control, average current control, and hysteresis control. The main objectives of the PFC converter are to draw sinusoidal input current and in phase with the input voltage, power quality improvement and lower THD of grid current, and stiff DC voltage at output. These power converters work in continuous conduction mode (CCM) and usually employ three sensors to accomplish PFC [27][28]. Fig. 2.4 presents different front-end PFC converters. These systems necessitate high

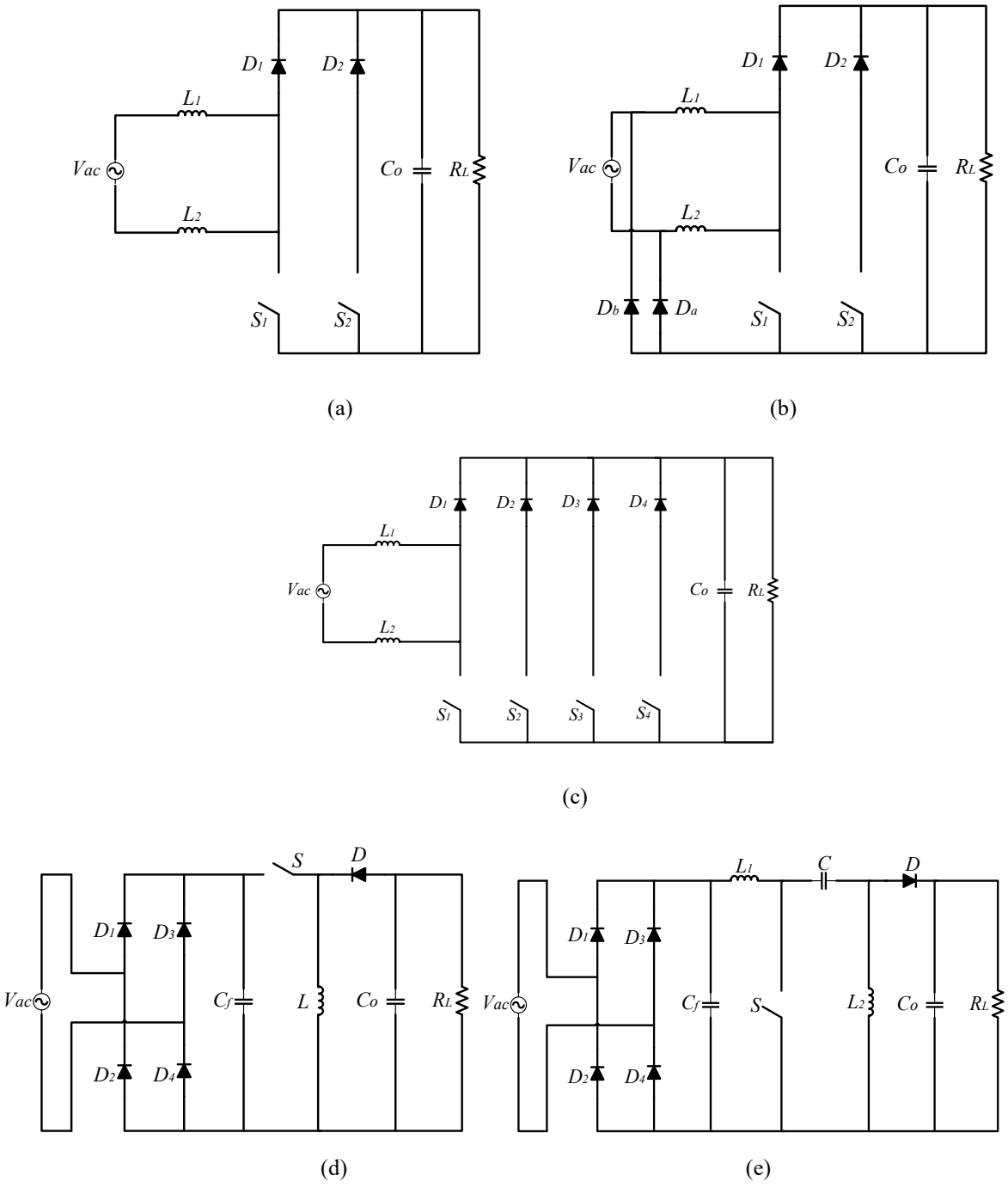

Fig 2.4. Frontend Converters; (a) Dual Boost PFC; (b) Phase Shifted Semi Bridgeless PFC; (c) Bridgeless Interleaved Boost PFC; (d) Conventional Buck-Boost PFC; (e) Sepic PFC;

sampling frequency for input current shaping. The second stage isolated DC-DC converter typically comprises of a switching network, transformer, rectifier, and a low pass filter. This stage converts the DC link voltage to a regulated DC voltage at the output as per the battery charger specifications requirement. The different categories of EV battery pack voltage range from 48V-

650V and the DC-DC converter used for the battery current control is usually a unidirectional buck converter, which steps down the voltage at the DC link to the battery voltage level. Fig. 2.5 shows few examples of the DC-DC converter employed in the second stage. An additional resonant tank maybe added for soft switching at high switching frequency of semiconductor devices and a high frequency transformer. It is advantageous to use a high frequency transformer than a line frequency transformer owing to size, cost, and weight [30].

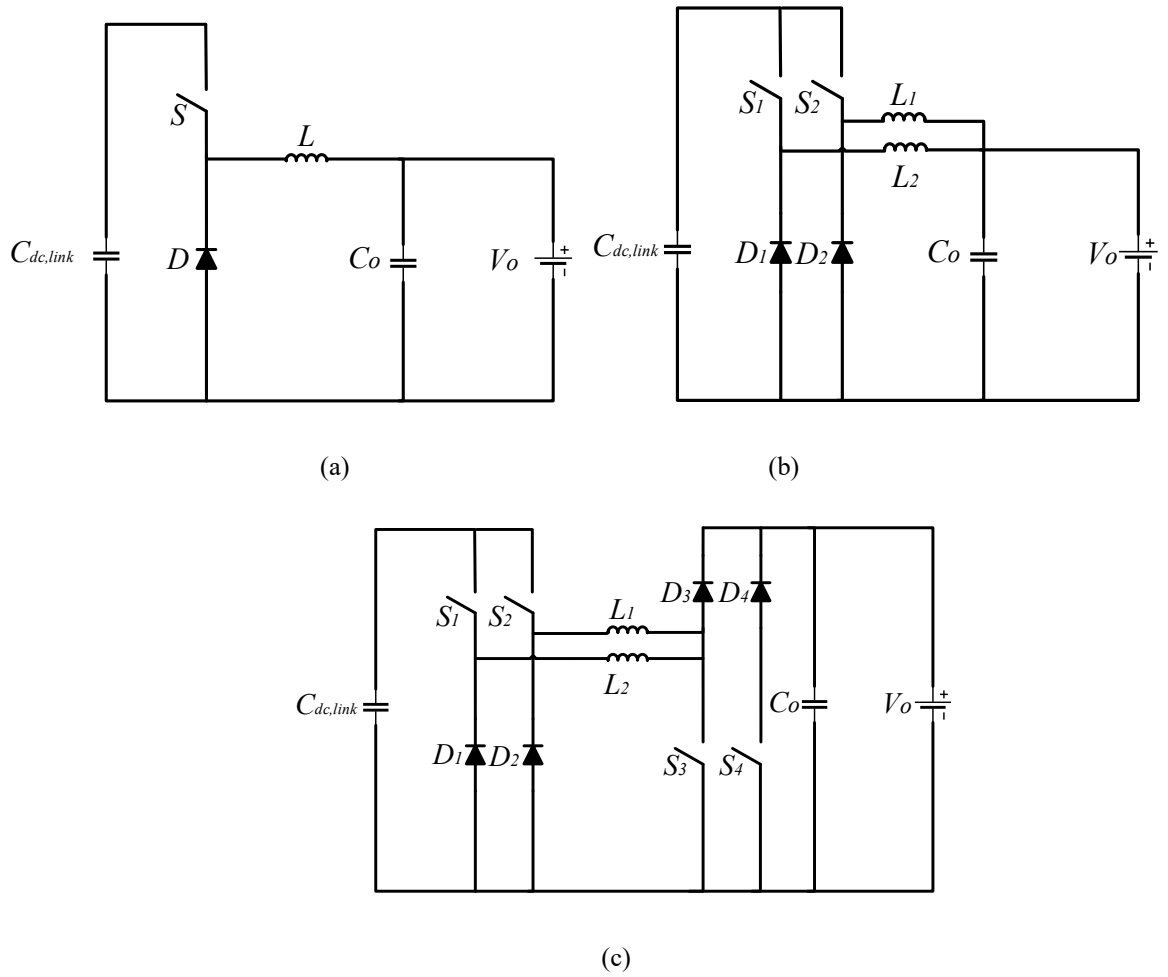

Fig 2.5. Backend Converter; (a) Buck Topology; (b) Interleaved Buck Topology; (c) Non Inverted Buck-Boost Topology;

The two most commonly used DC-DC converter configurations are the phase-shifted full-bridge (PSFB) converter [27] and LLC resonant converter [29][31] as shown in Fig. 2.6 (a) and (b), respectively. These topologies have issues of battery charge control. The PSFB converter by controlling the gating signals accomplishes the zero voltage switching turn-on of the primary side

switches but these converters lose ZVS at light load and thereby, the efficiency of the overall system is reduced [32]-[35]. However, LLC converters attain ZVS throughout the complete load range but to control the load voltage and current, these converters require complicated variable frequency modulation and a microcontroller with high clock rate, which reduces the reliability of the converter [36]-[39] as well as they have complex magnetics design. The two stage topology having galvanic isolation is a common topology with added safety measure but isolation is not a necessary requirement for the on-board battery chargers as per the standards [40][41]. The non-isolated topology can be suitably applied to the battery chargers and have more benefits than the single-stage and two-stage isolated topologies. These topologies have improved efficiency, and lower volume but they have higher semiconductor and sensor count, which makes the converter costly.

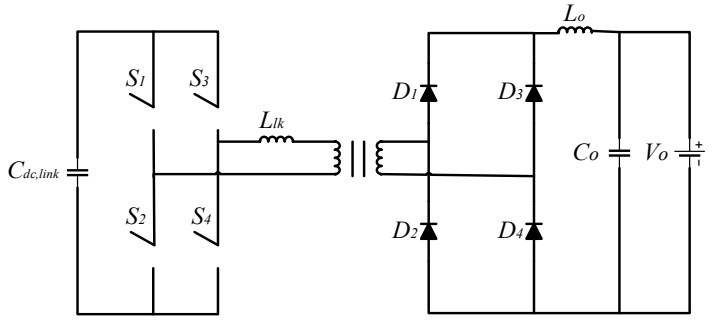

(a)

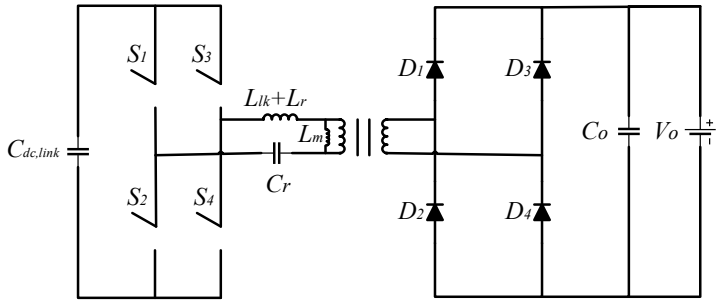

(b)

Fig 2.6. (a) Phase Shifted Full Bridge Topology; (b) Full Bridge LLC Resonant Topology;

2.4. Electric Vehicles Future Trends

EVs have not been extensively popular among public in spite of positive impact on the environment and high energy efficiency. One of the prime reasons is the lack of battery charging infrastructure, which requires a huge investment from the Government and the private sectors. The major barriers to infrastructure installations are codes and standards, costs of installation, planning of utility infrastructure, construction, knowledge of consumer, metering, role of contactor, permission procedures, etc. The charging infrastructure demand is based upon three factors namely; (a) penetration rates, (b) charging degree, and (c) range anxiety. Smart grid impacts on EV batteries and charging infrastructure is substantially uncertain.

In future, Level I and Level II slow EV charging are preferred schemes because of lower electricity rates and convenience. Charging at home will be crucial for accomplishing high EV usage rates. Public charging is more fundamental to move past the initial stages of EV adoption. Due to the non-requirement of wall box, this is the most economical infrastructure. But with battery capacity, EV range improvement, and potential requirement of Level III fast charging by EVs for range extension then there would be a higher requirement of building off-board charging station infrastructure. For passenger EVs, Level III fast charging reduces range anxiety. The high investment for fast charging infrastructure installation and the problems associated with large amount of energy transfer from the electricity grid assures that overnight and standard charging would be the prevalent methods for EV charging. For wide commercialization, the requirement of recharging in communities and highways is crucial. It is more probable that unidirectional charging would be the main aspect for development in the near future [42]. The basic attributes of unidirectional charging are listed in Table 2.2.

The successful EV adoption in the coming decade depends on the following:

a) Deployment of EV charging infrastructure is the primary consideration. The necessary parts consist of conductors, EV connectors, attachment plugs, device power outlets, apparatus installed for safe energy transfer.
b) Reliability, durability, and safety.
c) Reduced cost and higher efficiency.
d) Vehicle-to-grid (V2G) power flow, communication, and metering.

e) Accommodation of high-power charging.
f) Standardization of internationally agreed upon EV charging stations. Requirement of regulatory procedures and policies in the distribution market for commercial firms.
g) Ease in the charger and connector usage by the consumer.

Table 2.2: Attributes of Unidirectional Battery Charger

Attributes	Unidirectional EV Battery Charger and Infrastructure
Electric power flow and switches	Electric power flow in one way, Grid-to-Vehicle charging, diode bridge, and unidirectional converter
Availability	Available
Power level	Level 1, Level 2, and Level 3
Requirements	Power grid connection
Isolation	Isolated, and non-isolated
Control	Simple and charging current active control
Cost	Low cost and no added expense
Effect of battery	No degradation in discharging
Advantages	• Services of reactive power and dynamic adjustments of charge rates without reversal is provided • Supplies and absorbs reactive power even without discharging a battery by using current phase angle control • Control using voltage and frequency

2.5. Conclusion

This Chapter describes the EV battery charging classification concentrating primarily on the plug-in EV battery chargers. The basic attributes of the on-board and the off-board battery chargers are discussed. A comprehensive overview of the currently employed EV battery charging AC-DC converters along with their power quality limitations have been provided. This Chapter thoroughly discusses the recent trends in EV battery charger structure including the isolated and non-isolated topologies together with the single-stage and two-stage topologies. The disadvantages of flyback and half-bridge resonant single stage topologies involving low efficiency and higher component count has been discussed. The limitations of front-end diode bridge rectifier in terms of PFC operation has been explained. The two-stage configurations along with front-end and back-

end converter configurations are discussed. These converters operate in CCM and require at least three sensors and two control loops therefore, they increase the computational burden on the microcontroller. Sensors' count reduction makes the converter cost effective, lightweight, reliable, and robust. Different front-end and back-end battery charger topologies have been illustrated. Finally, the future EV trends and their successful deployment strategies have been discussed.

In the next chapter, a single phase bridgeless Cuk-derived AC-DC PFC converter as on-board EV charger is presented.

CHAPTER 3: SINGLE SENSOR BASED CUK DERIVED PFC CONVERTER FOR GRID TO VEHICLE CHARGING

3.1. Introduction

Increasing concerns regarding the environmental issues have immensely encouraged adoption of the electric vehicles (EVs) worldwide owing to their environmental friendly and pollution free operation. The EVs utilize high voltage batteries as their source of power and therefore, a charger is required for recharging the batteries. A typical EV battery charger block diagram is shown in Fig 3.1 [31]. The battery chargers are divided into two categories; a) on-board charger and b) off-board charger [43]. The on-board chargers (OBC) as represented in Fig 3.2 are mounted on the EV, thus it has to be compact in size as well as lightweight. Also, they are connected to the single-phase AC grid for the battery charging process. So, to meet the harmonic limits as required by standards [10], a power factor corrected (PFC) AC/DC converter becomes necessary at the front end of the AC supply.

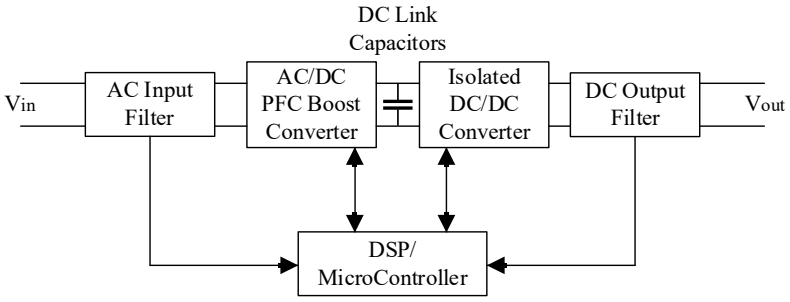

Fig 3.1. Block diagram for a typical battery charger

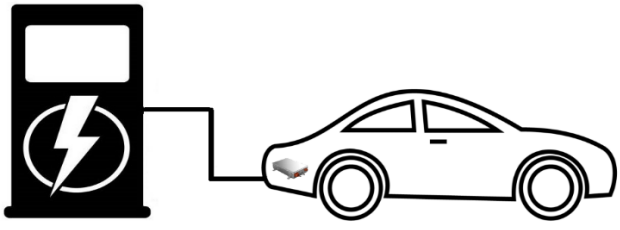

Fig 3.2. Grid to Vehicle (G2V) Charging using On-board EV Charger

Different PFC based charger topologies are reported in literature for OBC applications. The two-stage configuration [26][30[44]-[46] consists of a PFC converter and an isolated DC-DC converter in the first and second stage, respectively. This charger is easy to implement but has higher components' count, cost, and low density. The single stage configuration [17][31][47]-[52] is formed using a combination of a diode-bridge rectifier and a DC-DC converter. The input diode bridge rectifier contributes to high conduction losses. Thus, the bridgeless topologies [17][31][49]-[52] have been proposed, which removes the input diode bridge but still uses the same number of components. Therefore, this work proposes a novel single-phase bridgeless Cuk-derived front-end PFC converter with reduced components' count having simple control, which requires only a single loop and a single sensor.

3.2. Bridgeless Cuk-derived Topologies

The following bridgeless Cuk-derived topologies are derived from the conventional Cuk PFC converter as shown in Fig 3.3 [46]. The topology 1 (T1), topology 2 (T2), and topology 3 (T3) as reported are presented in Fig 3.4(a), Fig 3.4(b), and Fig 3.4(c), respectively [53].

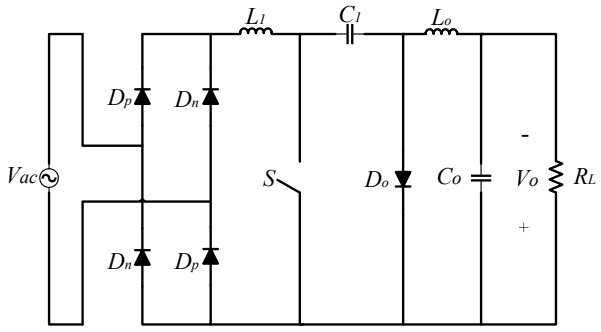

Fig 3.3. Conventional Cuk PFC converter

T1 has low input current, reduced EMI, and simple implementation but has the disadvantage of current circulation which contributes to extra losses in supply voltage which is the result of two intermediate capacitors interconnection. T2 has better thermal management however this configuration has higher component count. Additionally, T2 has an added floating terminal drawback as the load is located in between the two output capacitors. The switch arrangement adds an issue of floating neutral in the independent supply voltage half. Topology 3 (T3) has lower current stress and still incur losses because the inactive switch's 'S_2' body diode is always conducting in the positive half cycle through inductor 'L_2'. In the negative half cycle, the circuit

has some additional losses across the inactive switch body diode because of partial current flow return through it [46][53]. Fig 3.4 (d) and Fig 3.4 (e) [46] show two other bridgeless Cuk-derived topologies, which has same number of components and semiconductor device stress as conventional Cuk PFC converter. But these topologies have input and output

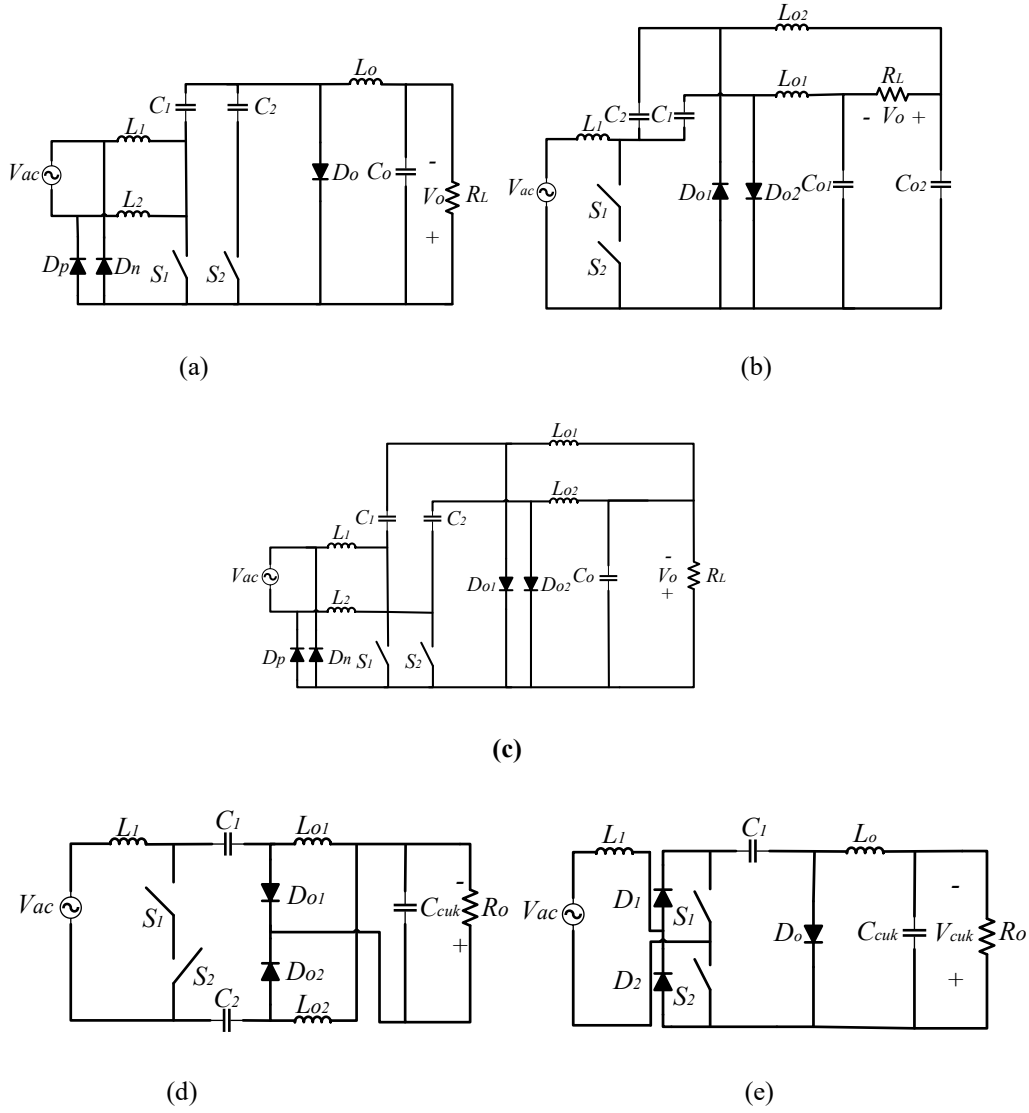

Fig 3.4. Bridgeless Cuk-derived Topologies; (a) BL-Cuk Topology 1 (T1) in [53] (b) BL-Cuk Topology 2, (T2) in [53] (c) BL-Cuk Topology 3 (T3) in [53] (d) BL-Cuk in [54] (e) BL-Cuk in [55]

inductor coupling issues which might result in high input and output ripple resulting in unsuitability for the service life of battery [54] [55]. Therefore, a novel bridgeless Cuk-derived converter with less components, and a simple control scheme compared to the prevailing topologies is introduced in this thesis. The output inductor in the proposed converter is designed

to operate in discontinuous current conduction mode for the entire converter power range to attain PFC naturally at the AC side, and as a result, source voltage and source current sensing is avoided, thereby decreasing the converter density, operational cost, and enhancing the converter robustness towards high-frequency noise. The proposed converter requires reduced number of components, and the voltage stress of the devices is lower in comparison to the conventional bridgeless Cuk PFC converter, which in turn reduces the switching-losses of the devices and boosts the overall converter efficiency.

3.3. Proposed Converter

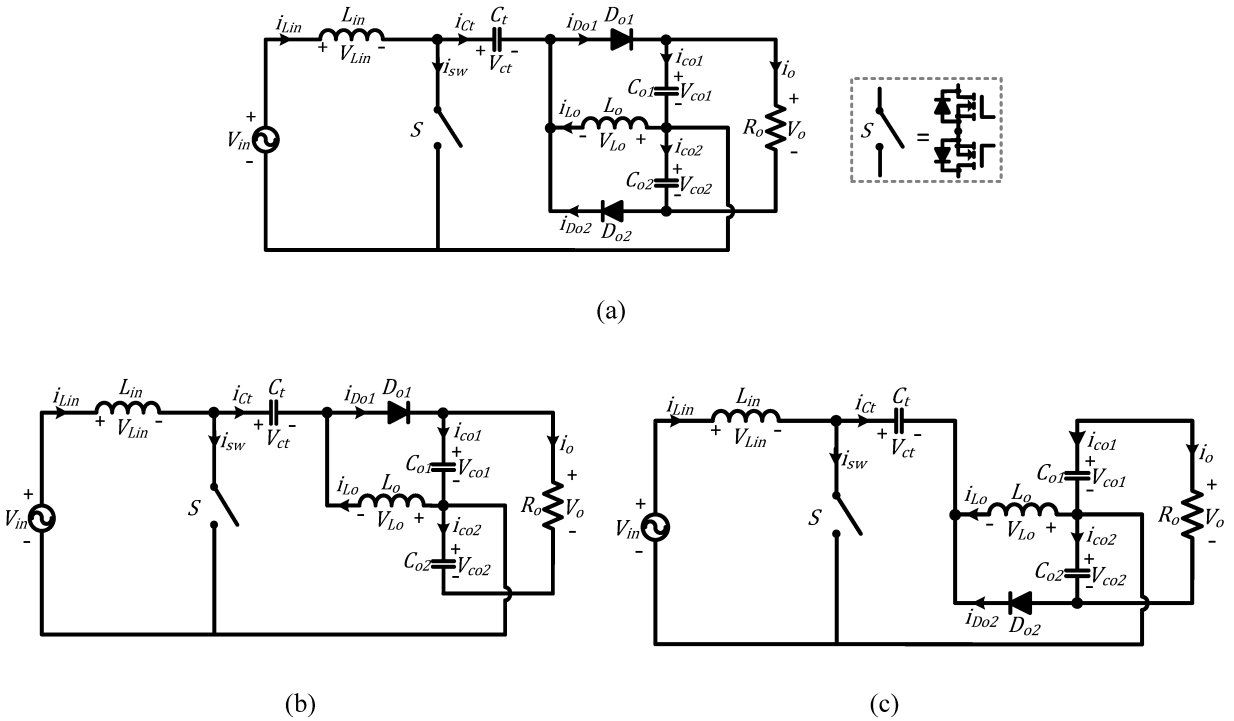

Fig. 3.5. (a) The proposed single-phase bridgeless Cuk-derived converter (b) BL Cuk configuration during positive half-cycles (c) BL Cuk configuration during negative half-cycles

The proposed AC-DC converter is derived from the conventional Cuk PFC converter and is presented in Fig. 3.5(a). The proposed converter has lower components' count. The total number of switches are four (two MOSFETs and two diodes) in the proposed converter whereas the convention Cuk PFC has six switches (one MOSFET and five diodes). The topology consists of a bidirectional switch, diodes, inductors, and capacitors. The bidirectional switch provides bidirectional blocking capability and is counted as one because it is setup by joining two

MOSFETs back-to-back and the same PWM gating signal is used to operate. The voltage doubler aids in AC-DC conversion. The total number of components is eight in the proposed converter whereas the conventional Cuk converter has ten components. Fig. 3.5(b) and Fig. 3.5(c) describes the converter configuration in positive and negative half cycle, respectively. Diode 'D_{o1}' operates in positive half cycle and the diode 'D_{o2}' operates in negative half cycle. The converter operates in such a way that throughout the converter operation either the bidirectional switch or any of the diodes will be in the current conduction path. Thereby, resulting in reduction of the conduction losses as well as making the converter thermal management easy. Also, the semi-conductor voltage stress which is ($V_{pk} + \frac{V_o}{2}$) is lower as compared to the voltage stress, which is (V_{pk} + V_o) in the conventional Cuk converter thereby, decreasing the switching losses and increasing the operating efficiency of the converter. The proposed converter is designed to operate in DCM to obtain PFC naturally at the AC side thereby, the control loop and sensor's count are reduced to one.

3.4. Steady State Analysis

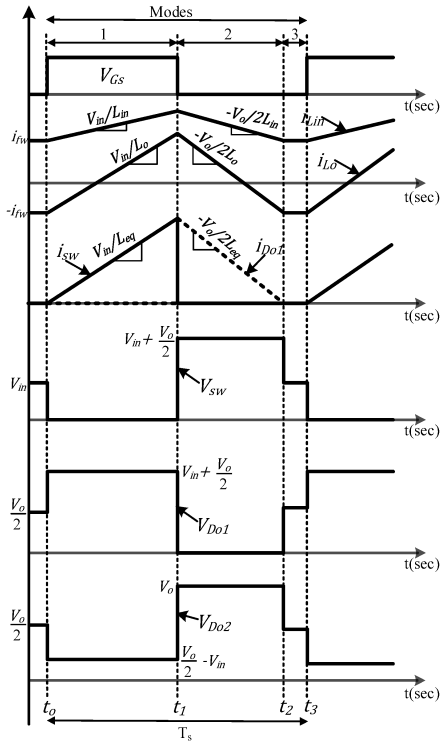

Fig. 3.6. The proposed BL-Cuk converter waveforms for one switching cycle during positive half-cycle

The steady state operation over one switching cycle is explained in this Section. Due to the symmetric operation of the converter, the operation in the positive half cycle is described here. The key waveforms for the converter operation description during positive half cycle over one switching cycle is presented in Fig 3.6. The discontinuous output diode current proves the DCM operation of the converter throughout the power range. The converter operation has three modes in one switching cycle as presented in Fig 3.7 with their equivalent circuits.

The following assumptions are made to understand the steady state analysis and operation of the converter:

a) The components are assumed ideal and lossless.
b) The output filter capacitor is large enough to maintain constant output voltage.
c) C_{o1} C_{o2} share output voltage equally.
d) The transfer capacitor 'C_t' has average voltage equal to the input voltage.
e) As switching frequency is very high compared to the supply frequency; the source voltage, output capacitor voltage and voltage across transfer capacitor are considered constant in one switching cycle.

Converter Operation Description:

Mode 1 (t_o – t_1): When the switch 'S' is turned ON, this mode begins. Prior to this mode, the input current 'i_{Lin}' is represented as 'i_{fw}' freewheels in the loop formed by 'V_{in}' 'L_{in}' 'C_t' and 'L_o' as shown in Fig 3.6. The equivalent circuit of operation is depicted in Fig 3.7(a). In this mode, the source 'V_{in}' supplies energy to the input inductor 'L_{in}' and the transfer capacitor 'C_t' supplies energy to the output inductor 'L_o' with a slope of $\frac{V_{in}}{L_{in}}$ and $\frac{V_{in}}{L_o}$, respectively.

$$i_{Lin} = i_{fw} + \frac{V_{in}}{L_{in}}t \tag{3.1}$$

$$i_{Lo} = -i_{fw} + \frac{V_{in}}{L_o}t \tag{3.2}$$

Mode 2 (t_1 – t_2): This mode begins when the switch 'S' is turned off. Before this mode initiates, the currents through input and output inductor has reached their maximum values. The complete switch current is carried by the 'D_{o1}' output diode when the switch is turned off and is represented in Fig 3.6. Fig 3.7(b) shows the converter operation equivalent circuit during this

mode. The input and output inductor demagnetization takes place in this mode by transferring the stored energy to the load but the output capacitor 'C_{o1}' and transfer capacitor 'C_t' are getting charged.

$$i_{Lin} = i_{fw} + \frac{V_{in}}{L_{in}} DT_s - \frac{V_o}{2L_{in}} t \tag{3.3}$$

$$i_{Lo} = -i_{fw} + \frac{V_{in}}{L_o} DT_s - \frac{V_o}{2L_o} t \tag{3.4}$$

where $DT_s = T_{on}$ which is the conduction time of the switch. This mode ends when the diode 'D_{o1}' current becomes zero.

$$i_{Lin} + i_{Lo} = 0 \tag{3.5}$$

Solving (3.5), the following expression is obtained

$$D_1 T_s = \frac{2V_{in}}{V_o} DT_s \tag{3.6}$$

where $D_1 T_s$ represents mode 2 time duration.

Mode 3 ($t_2 - t_3$): In this mode, the load is being supplied by the output capacitors where all the semiconductors are OFF. The equivalent circuit is shown in Fig 3.7(c).

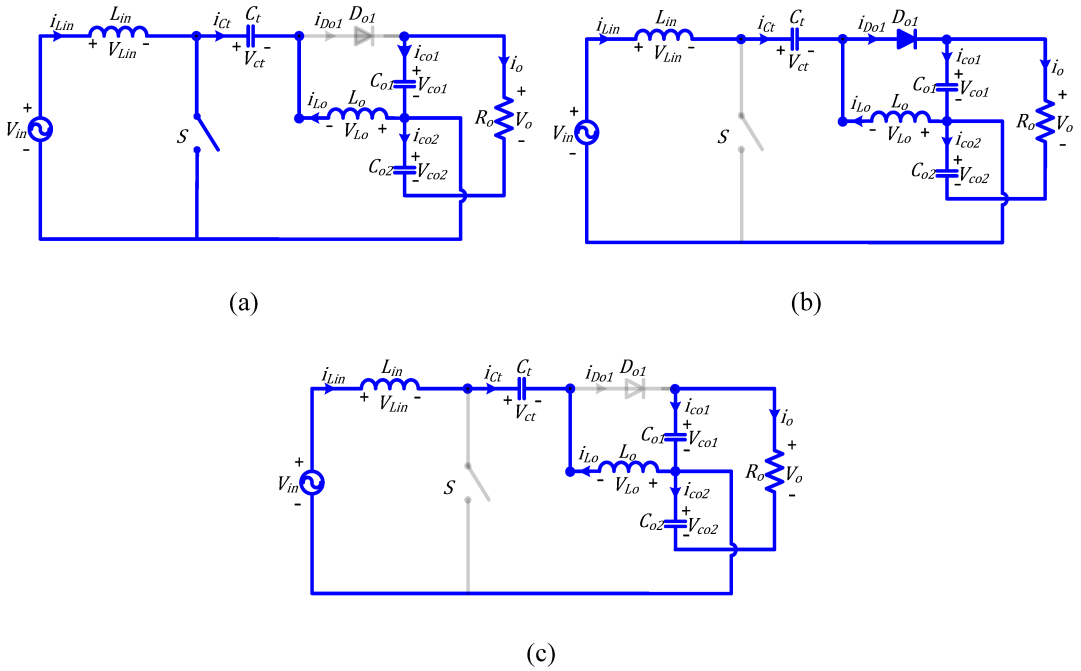

Fig. 3.7. Proposed BL-Cuk converter equivalent circuits; (a) Mode-1; (b) Mode-2; (c) Mode-3.

3.5. Converter Design

The following section provides the detailed design procedure of the bridgeless Cuk-derived converter.

3.5.1. DCM Operation Condition

The condition for DCM operation of the converter is

$$DT_s + D_1T_s \leq T_s \tag{3.7}$$

$$D \leq \frac{M}{M+2sin\omega t} \tag{3.8}$$

where $V_{in} = V_{pk} \sin\omega t$ and $M = \frac{V_o}{V_{pk}}$

In (3.8), the worst case scenario is when $\sin\omega t = 1$ that implies to $\omega t = \frac{\pi}{2}$. So, the DCM operation condition becomes

$$D \leq \frac{M}{M+2} \tag{3.9}$$

From (3.9), the critical value of the voltage conversion ratio for a specific duty cycle is

$$M_{cr} \geq \frac{2D}{1-D} \tag{3.10}$$

where M_{cr} = critical voltage conversion ratio. The output voltage of the converter must be twice as high as the peak input voltage such that output diodes are reverse biased, which is evident from the converter configuration. So, for the proposed converter operation, to work correctly the voltage gain should be

$$M \geq M_{cr} \geq 2 \tag{3.11}$$

3.5.2. Average Output Current

The average output current of the converter for one switching cycle is equal to the average output diode 'D_{o1}' current. The shape of output diode current is triangular and the average of it can be determined by

$$I_{Do1,avg} = \frac{i_{Do1,pk}D_1T_s}{2T_s} \tag{3.12}$$

where $i_{Do1,pk} = \frac{V_{in}}{L_{eq}} DT_s$, $L_{eq} = \frac{L_{in}L_o}{L_{in}+L_o}$ and $i_{Do1,pk}$ stands for peak output diode 'D_{o1}' current.

Solving (3.12),

$$i_{Do1,avg} = \frac{V_{pk}^2 D^2 T_s}{L_{eq} V_o} \sin^2 \omega t \tag{3.13}$$

The average diode output current 'D_{o1}' over a line period is

$$i_{Do1,avg} = \frac{V_{pk}^2 D^2 T_s}{4\, L_{eq} V_o} \tag{3.14}$$

3.5.3. Passive Components Design of Converter

The design of input inductor is done based on the peak input current ripple through a switching cycle. The peak input inductor current ripple (Δi_{Lin}) is

$$\Delta i_{Lin} = \frac{V_{pk}}{L_{in}} DT_s \tag{3.15}$$

$$L_{in} = \frac{V_{pk}}{\Delta i_{Lin}} DT_s \tag{3.16}$$

'L_o' is given by

$$L_o = \frac{L_{in}L_{eq}}{L_{in}-L_{eq}} \tag{3.17}$$

'L_{eq}' is derived using (3.9) and (3.14), and is given by

$$L_{eq} \leq \frac{V_{pk}^2 {V_o}^2 T_s}{4\, P_{out}(V_o+2V_{pk})^2} \tag{3.18}$$

where P_{out} = rated output power of converter

The output capacitor in single phase PFC converter is designed to filter out the second order harmonics of supply frequency which are visible in the output voltage. Taking $C_{o1} = C_{o2} = C_o$, the low frequency ripple of output voltage is

$$\Delta V_{o,ripple} = \frac{1}{C_o}\left(\int i_{co_1} dt + \int i_{co_2} dt\right) \tag{3.19}$$

$$\Delta V_{o,ripple} = \frac{1}{C_o}\left(\int i_{D_{o1},avg} - 2i_o\right) dt \tag{3.20}$$

$$= \frac{2i_o}{\omega C_o} \tag{3.21}$$

$$C_o = \frac{2i_o}{\omega_{\Delta Vo,ripple}} \tag{3.22}$$

The transfer capacitor 'C_t' is critical because the input current quality is highly influenced by its value. The value should be chosen in a way that it does not result in low frequency oscillations with both input and output inductors. Therefore, the resonant frequency 'f_{res}' for the transfer capacitor 'C_t' must be between the value of switch and supply frequency.

$$f_{in} << f_{res} << f_s \tag{3.23}$$

where f_{in} is defined as input supply frequency, f_s as switching frequency and

$$f_{res} = \frac{1}{2\pi\sqrt{C_t(L_{in}+L_o)}} \tag{3.24}$$

3.6. Small Signal Modeling

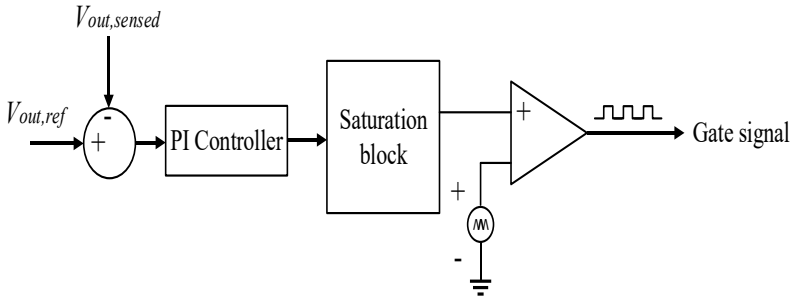

Fig. 3.8. Output voltage controller configuration

The design of the converter is in discontinuous inductor current conduction mode to attain the PFC naturally at the AC input thereby, avoiding the input voltage and current sensing. Therefore, only one voltage control loop is required as shown in Fig. 3.8. A straightforward approach known as 'Current Injected Equivalent Circuit Approach' is used to develop the control-to-output voltage transfer function of the converter [56]. The modeling based on this technique is very simple and easy to comprehend. The fundamental idea of this method is linearization of the non-linear part of the power converter by putting the average output current over a line period in its place, which is shown in Fig. 3.9. The perturbation in output voltage can be represented as (3.25).

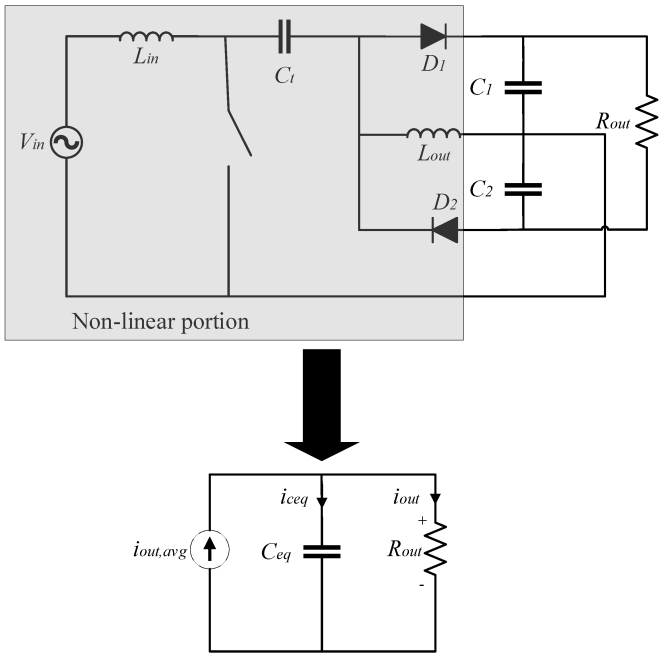

Fig. 3.9. Equivalent circuit model of the power converter for small signal analysis

$$\widehat{Vout} = \widehat{Iout,avg} * \frac{R}{1+sRC} \tag{3.25}$$

Perturbing I_m and $I_{out,avg}=\frac{V_m^2 D^2 T_s}{4LV_o}$, (3.26) and (3.27) are obtained. Fig 3.10 represents the small signal model of the converter.

$$\widehat{I_m} = i_1\widehat{D} + \frac{\widehat{V_m}}{r_1} \tag{3.26}$$

$$\widehat{I_{out,avg}} = i_2\widehat{D} + g_2\widehat{V_m} - \frac{\widehat{V_{0ut}}}{r_2} \tag{3.27}$$

where $i_1 = \frac{V_m D T_s}{L}$, $r_1 = \frac{2L}{T_s D^2}$, $i_2 = \frac{V_m^2 D T_s}{2LV_{0ut}}$, $g_2 = \frac{V_m D^2 T_s}{2LV_{0ut}}$, $r_2 = \frac{V_o}{I_o}$. Using (3.27) in (3.25) and equating $\widehat{V_m} = 0$, the required control to output voltage transfer function is obtained in (3.28).

$$\frac{\widehat{V_o}}{\widehat{D}} = \frac{DV_m}{2K_{cond}M(1+sRC_{eq})} \tag{3.28}$$

where $= \frac{V_o}{V_m}$, $K_{cond} = \frac{2L}{RT_s}$, $C_{eq} = \frac{C_1 * C_2}{C_1 + C_2}$.

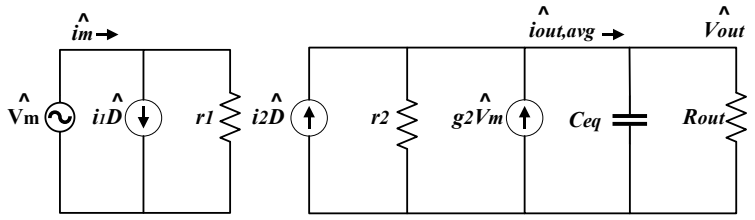

Fig. 3.10. Small signal model

3.7. Results and Discussions

This Section provides the detailed discussions about the simulation and experimental results.

3.7.1. Simulation Results

The modeling and simulation of the converter as shown in Fig 3.5(a) is done in PSIM 11. The specifications and the design values are listed in Table 3.1 and Table 3.2, respectively. Using the design parameters in (3.28), the plant transfer function is obtained in (3.29). For attaining the required system response, a PI controller ($\frac{K_i}{s} + K_p$) is employed, which is sufficient as the plant transfer function is only a single pole system. The tuning of the controller is done using MATLAB Sisotool having phase margin (PM) of 60 degrees and a bandwidth having value less than 754 rad/s. The PM of 60 degrees has a corresponding damping of 60 percent and 10 percent overshoot.

Table 3.1: Input Specifications

Parameter	Value
Input Voltage (V_{in} (rms))	120V
Output Voltage (V_o)	400V
Output Power (P_o)	1kW
Output Voltage Ripple ($V_{o,\ ripple}$)	2%
Input Current Ripple ($I_{in,\ ripple}$)	8%
Switching Frequency (f_{sw})	50kHz
Line Frequency (f_{line})	60Hz

The obtained transfer function is given in (3.30). The value of k_p (=0.0062) and k_i (=0.28286) can be derived from (3.30). The capability of the system for tracking the reference DC with zero steady-state error can be implied from the open loop transfer function in (3.31), which has a gain of infinity for lower frequencies. Also, the robustness towards source voltage and load change disturbance is confirmed.

Table 3.2: Design Parameters

Parameter	Value
Maximum Duty Cycle (D_{max})	0.541
Input Inductor (L_{in})	1.5 mH
Output Inductor (L_o)	29 µH
Transfer Capacitor (C_t)	2.3 µF
Output Cpacitor (C_{o1}, C_{o2})	1.66 mF

Fig. 3.11 shows the bode plot of plant transfer function, controller transfer function, and open loop transfer function. The Hall-effect sensor LV25-P is used to sense the output voltage. The designed controller is implemented by coding the TI-DSP-TMS320F28335 to generate the gating signals of the switches of the converter, which is done by comparing the actual voltage with the reference voltage and the resulting error is fed to the proportional integral (PI) controller; the controller output is compared with the 50 kHz sawtooth waveform.

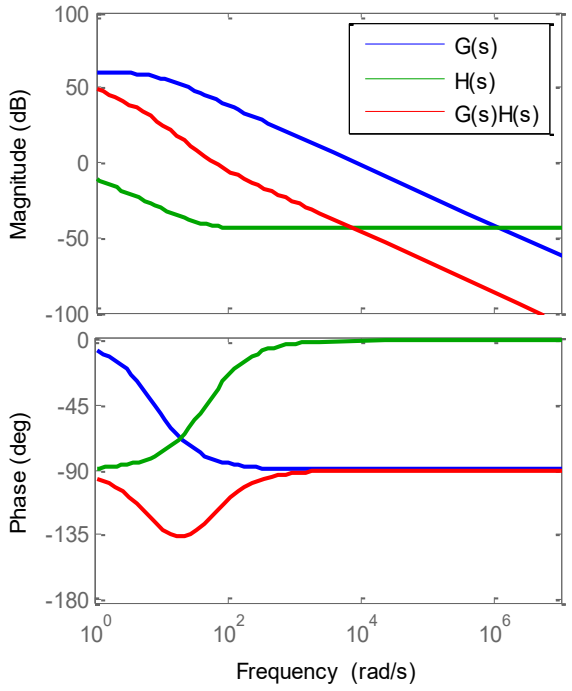

Fig. 3.11 Bode plot of G(s), H(s), and G(s)*H(s)

$$G(s) = \frac{V_o(s)}{D(s)} = \frac{1030}{0.133s+1} \tag{3.29}$$

$$H(s) = \frac{0.28286}{s} + 0.0062 \tag{3.30}$$

$$G(s) * H(s) = \frac{1030*(0.28286+0.0062s)}{s(0.133s+1)} \tag{3.31}$$

As a result, the switch's PWM signals are generated. To stop the power converter from reaching CCM as well as to protect against overloads, a limiter is placed. Increasing the switching frequency would reduce the size of the passive components but will increase the switching losses of the semiconductor devices, which in turn will reduce the overall efficiency of the converter requiring increased cooling requirement. Since this converter is AC-to-DC and hard switching therefore, it is not preferred to operate the semiconductor devices at a very high switching frequency due to noise and efficiency concerns. Thus, an optimum switching frequency of 50 kHz is selected without compromising much on the size, weight, cost, and efficiency of the converter. Fig 3.12(a) shows that the input current is exactly following the input voltage both in shape and the phase, which proves the unity power factor operation of the proposed converter at full-load condition. The output voltage and current at the rated output are demonstrated in Fig 3.12(b).

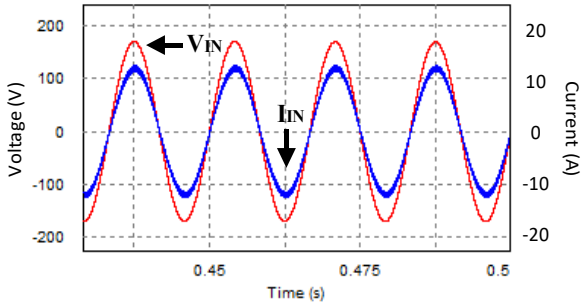

(a)

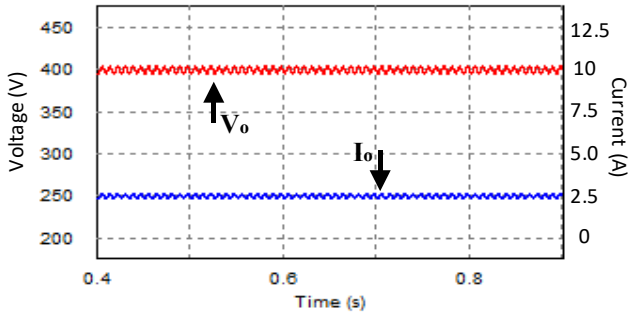

(b)

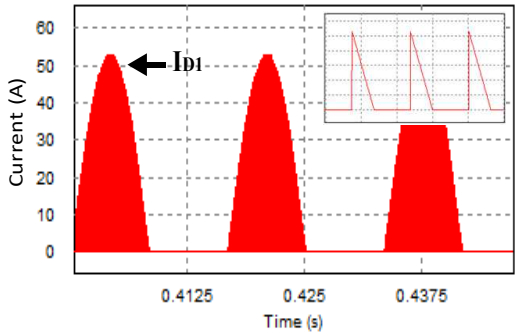

(c)

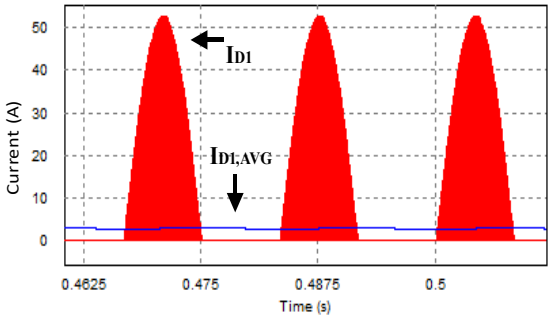

(d)

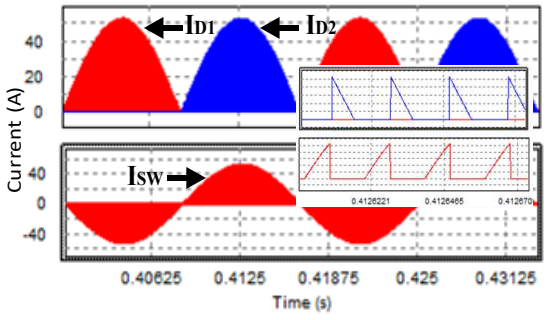

(e)

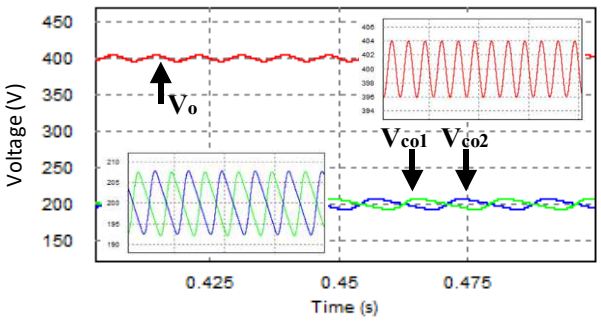

(f)

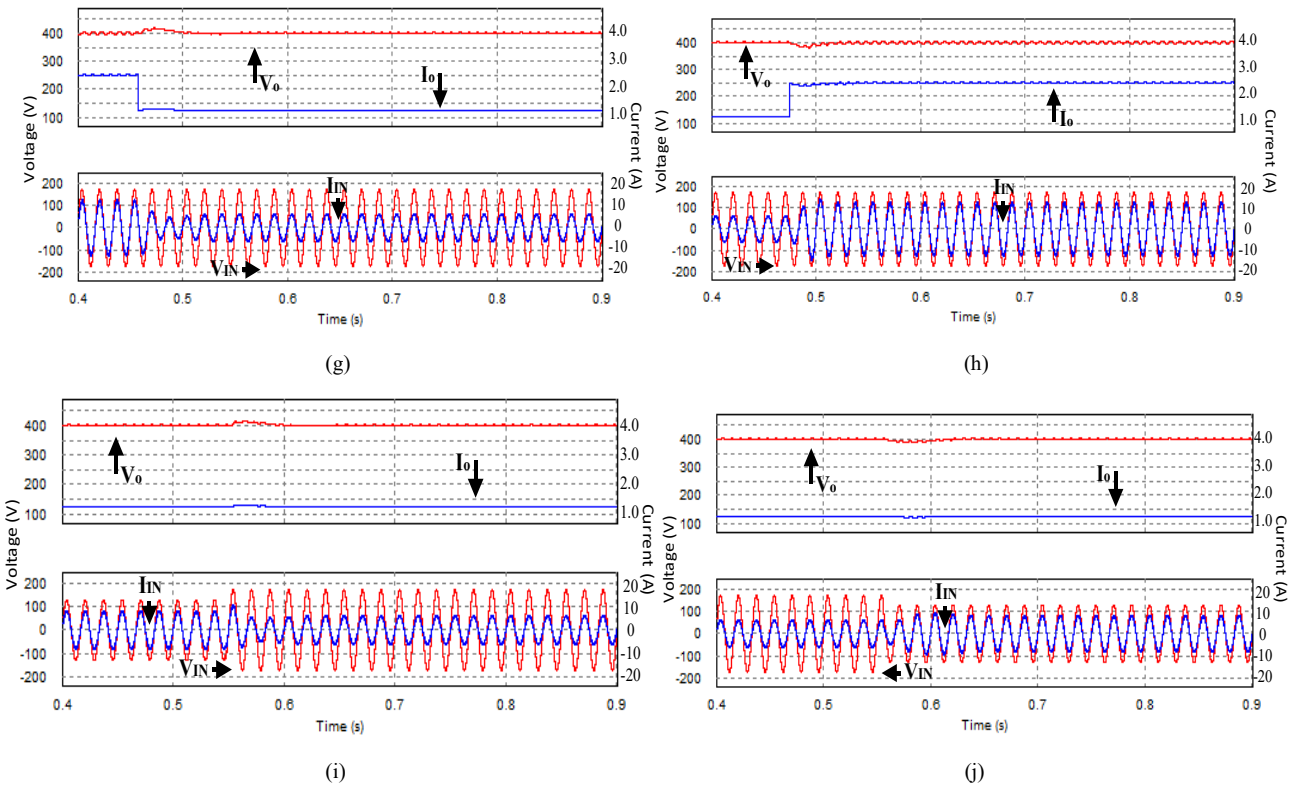

Fig. 3.12. Simulation results (a) source voltage and source current; (b) output voltage and current; (c) diode 'D_{o1}' current ; (d) diode 'D_{o1}' current and its mean current; (e) output diodes current and switch current; (f) output capacitor voltage and output voltage; (g) Load change from 1kW to 500W; (h) Load change from 500W to 1kW; (i) Source voltage change from 90V to 120V; (j) Source voltage change from 120V to 90V

The discontinuous output diode current 'I_{Do1}' in Fig 3.12(c) validates the converter design. Fig 3.12(d) shows the average diode current and output current are equal confirming the analysis. Fig 3.12(e) depicts the switch and output diode current, which makes the fact obvious that the current flow path has only one semiconductor device for the entire converter operation. The voltage across output capacitor sharing half of the voltage at the output are shown in Fig 3.12(f). Also, it depicts that the total output voltage ripple is half compared to the voltage ripple of the output capacitors. The output voltage settles at 400V exactly having peak to peak voltage ripple of 8V which is 2% as designed, thereby, aligning with the analysis. Fig. 3.12(g) and Fig. 3.12(h) show the response when the load is perturbed from 1kW to 500W and from 500W to 1kW, respectively. It is evident from Fig. 3.12(g) and Fig. 3.12(h) that the output voltage tracks the reference voltage appropriately and settles within 30ms. In Fig. 3.12(i) and Fig. 3.12(j), the input voltage is perturbed by 25% increment and decrement to test the controller's stability. The PFC operation is verified in all cases.

3.7.2. Experimental Results

A hardware prototype rated at 1kW as shown in Fig 3.13. is developed in the laboratory for the purpose of analysis and design validation of the proposed converter. Components used to build the hardware prototype are listed in Table 3.3. For designing the input inductor, the worst case voltage scenario and a peak input current ripple of 8% is considered.

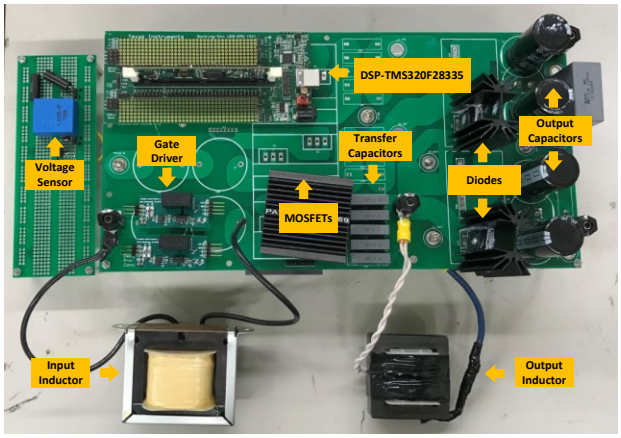

Fig. 3.13. Experimental hardware prototype of the proposed BL-Cuk PFC converter

All the steady-state output waveforms of the proposed converter are shown in Fig 3.14. The UPF operation at full- load and light-load are shown in Fig. 3.14(a) and Fig. 3.14(b), respectively. Moreover, the input current FFT analysis at 1kW is presented in Fig. 3.14(j). Table 3.4 lists the measured THD of the input current as well as power factor at different values of output power. The transfer capacitor voltage follows the input voltage and the average voltage of transfer capacitor is equal to the voltage at the input, which is represented in Fig. 3.14(c) and makes assumption (d) evident. Fig. 3.14(d) confirms when one diode is conducting and the other one is

Table 3.3: Experimental Hardware Prototype Components Specifications

Component	Specifications
MOSFET	UJ3CO65030K3S, SiC, 650 V, 35 mΩ
Diodes	60EPF12, 1200 V, 60 A
Input Inductor (Lin)	159ZL-C14H, 1.8 mH at 50 kHz
Output Inductor (L_O)	E 55/28/21 Ferrite core, 29 µH
Transfer Capacitors (C_t)	R71PI34704030M, 0.47µF*5
Output Capacitors (C_{O1}, C_{o2})	ESMQ401VSN471MQ50W,470 µF*3
DSP	TMS320F28335
Gate Driver	IC- IXYS-IXDN609SI
Power Source	California Instruments AST1503
Voltage Sensor	LV25-P

in blocked mode. The zoomed version of the back-to-back connected switch voltage is shown in Fig. 3.14(e) and the peak voltage stress is 370V that is about ($V_{pk} + \frac{V_O}{2}$), which agrees with the analysis. D_{o1} conducts during positive half cycle and D_{o2} conducts during negative half cycle and that is seen in Fig. 3.14(f) which confirms that only one semiconductor is in current conduction path. Fig. 3.14(g) demonstrates that the output voltage is twice the input voltage peak so that the output diodes can be reverse biased to operate the converter as intended. Fig. 3.14(h) shows the zoomed output inductor current which is designed to operate in DCM mode. The output voltage is shared equally between the output capacitors and the output voltage has half the voltage ripple as compared to the output capacitors as seen in Fig 3.14(i) and validating assumption (c). Despite the DCM design, which results in high peak current, a high efficiency of 94% is achieved.

Table 3.4: Input Current THD and Power Factor

Power Output (W)	THD (%)	PF
250 W	3.88	.9992
500 W	3.73	.9993
800 W	3.54	.9994
1000 W	3.49	.9994

Fig. 3.14(k) and 3.14(l) present the power converter response for the load change from 500W to 1kW and from 1kW to 500W, respectively. In Fig. 3.14(k), the power enhances by the current increment whereas in Fig. 3.14(l), the power is reduced by the current decrement. The output voltage is tracking the reference voltage appropriately and the settling time is as designed of 30ms.

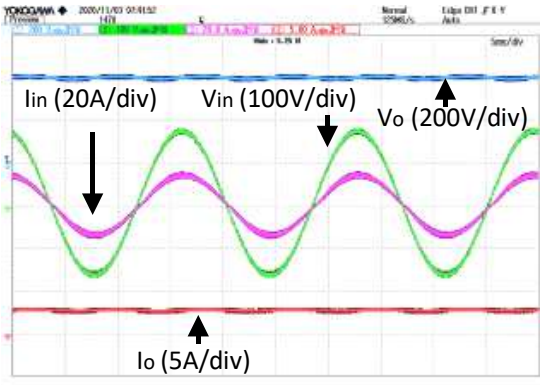

(a)

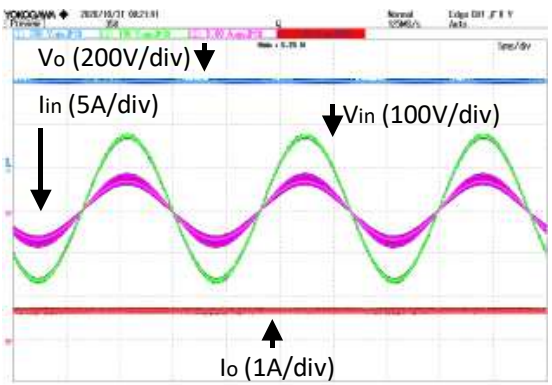

(b)

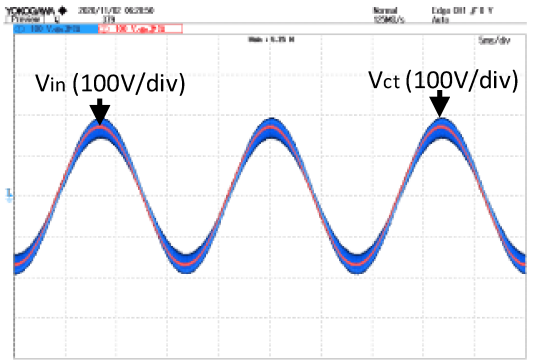
Vin (100V/div)
Vct (100V/div)

(c)

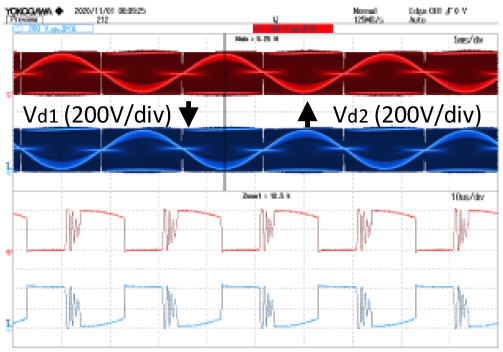
Vd1 (200V/div)
Vd2 (200V/div)

(d)

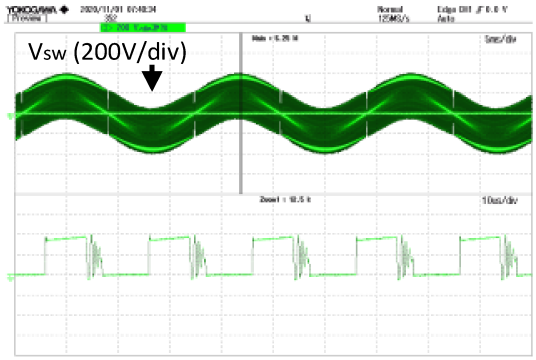
Vsw (200V/div)

(e)

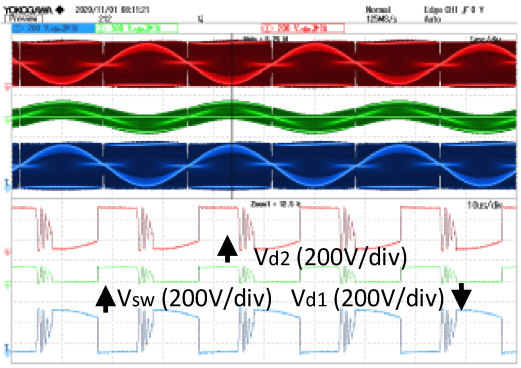
Vd2 (200V/div)
Vsw (200V/div)
Vd1 (200V/div)

(f)

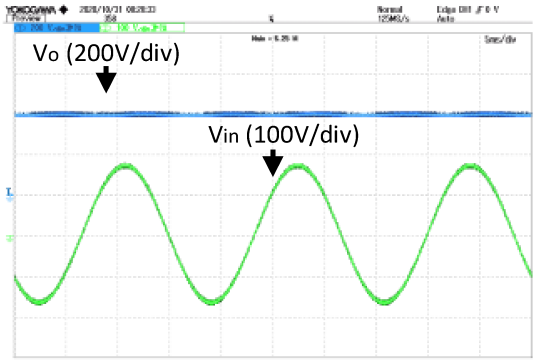
Vo (200V/div)
Vin (100V/div)

(g)

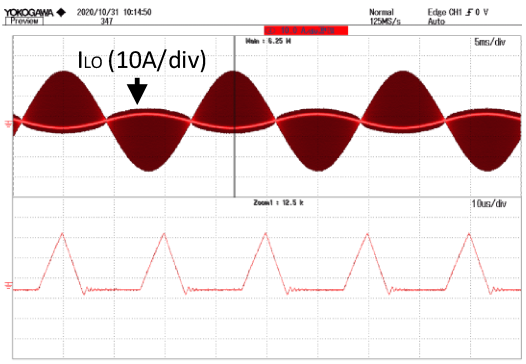
ILO (10A/div)

(h)

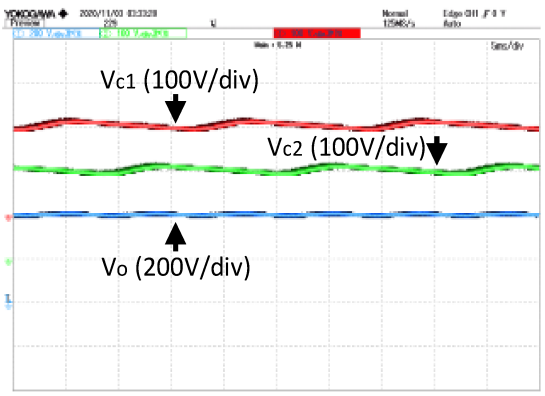
Vc1 (100V/div)
Vc2 (100V/div)
Vo (200V/div)

(i)

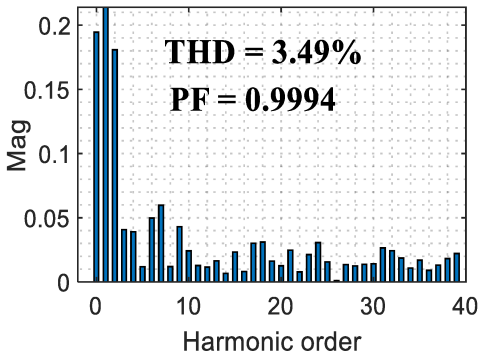
THD = 3.49%
PF = 0.9994
Mag
Harmonic order
0.2
0.15
0.1
0.05
0
0
10
20
30
40

(j)

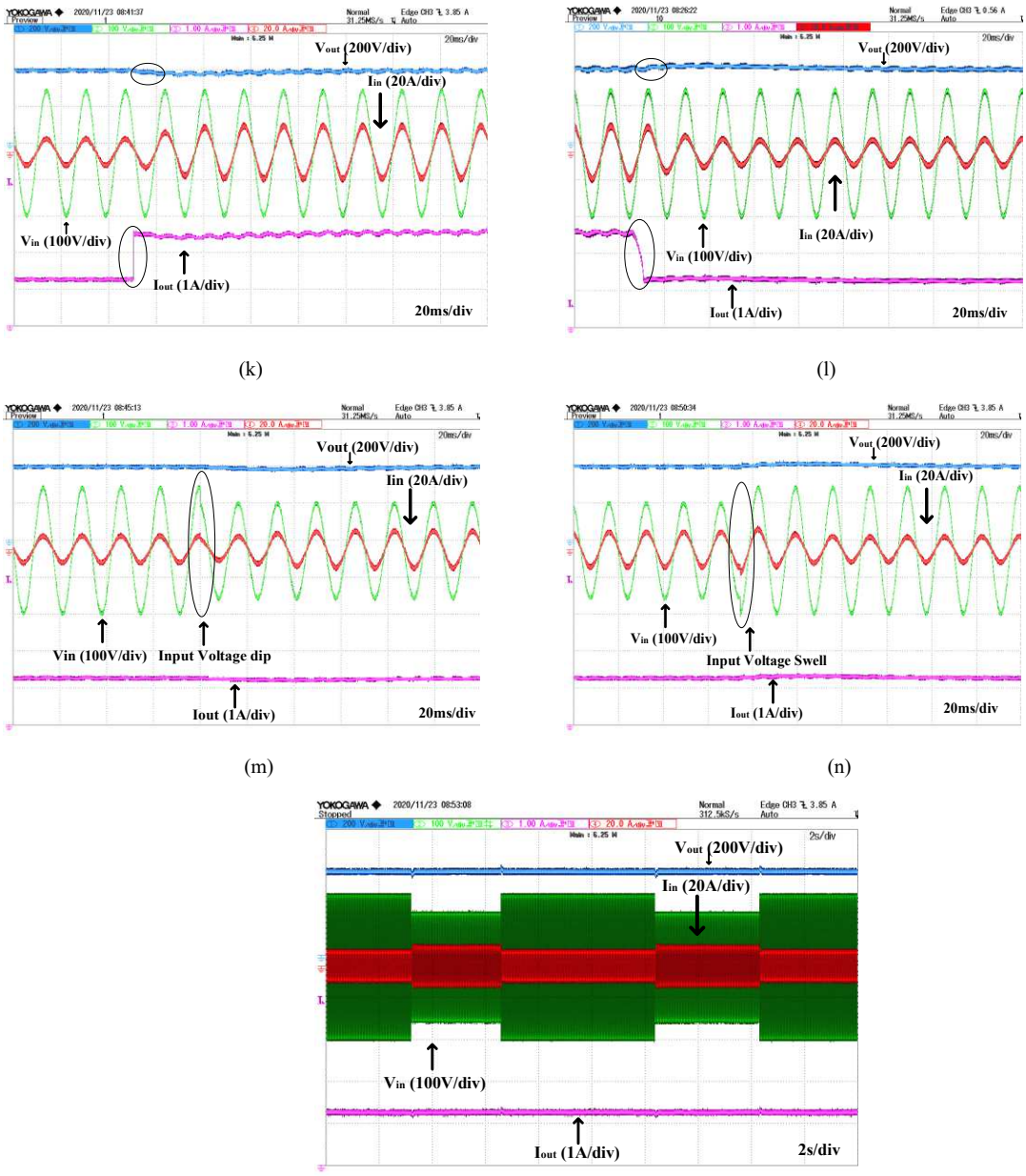

Fig. 3.14. Experimental results (a) PFC operation and output voltage and output current at 1kW; (b) PFC operation and output voltage and current at 25% load; (c) Voltage across intermediate capacitor at 500W; (d) Diode 'D_{o1}' and 'D_{o2}' voltage; (e) Bidirectional switch voltage; (f) HF output diodes and switch voltage; (g) Source voltage and output voltage; (h) Output inductor current at 50% load; (i) Output capacitors voltage and output voltage at 80% load; (j) FFT analysis of source current; (k) Load change from 500W to 1kW;(l) Load change from 1kW to 500W;(m) Source voltage change from 120V to 90V;(n) Source voltage change from 90V to 120V; (o) Source voltage change 120V-90V-120V-90V-120V;

In Fig. 3.14(m) and Fig. 3.14(n), the input voltage is perturbed by subjecting it to 25% voltage dip and voltage swell condition to verify the controller's robustness. In the voltage dip condition, it is observed that the current at the input rises to maintain same power. On the other hand, during

voltage swell condition, the input current falls to maintain the equal power. To further validate the robustness of the controller in Fig. 3.14(o), the source voltage is perturbed consecutively from 120V-90V-120V-90V-120V. It should be noted that the PFC operation is maintained in all cases. Fig. 3.15 shows the variation of PF with power level and Fig. 3.16 shows the variation of THD with power level graphically to identify the trend. Table 3.5 shows the comparison of different bridgeless topologies with the proposed converter.

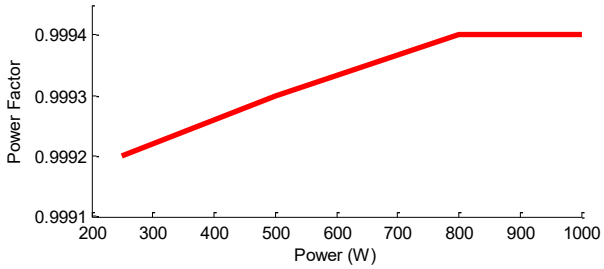

Fig. 3.15. PF Vs power graph

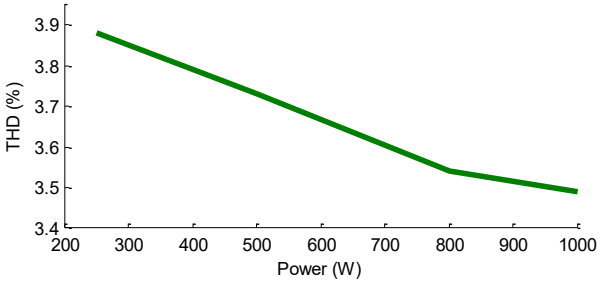

Fig. 3.16. THD Vs power graph

Table 3.5: Comparison of Different Bridgeless Configurations

Configuration	**BL-Boost [31]**	**BL-Buck Boost [57]**	**BL-Sepic [58]**	**BL-Zeta [59]**	**BL-Cuk T1[53]**	**BL-Cuk T2[53]**	**BL-Cuk T3[53]**	**BL-Cuk [54]**	**BL-Cuk [55]**	**Proposed**
Component Count	13	11	11	9	11	11	13	10	10	8
Diodes	4	4	3	3	3	2	4	2	3	2
Inductors	4	3	3	2	3	3	4	3	3	2
Intermediate Capacitor	0	0	2	1	2	2	2	2	1	1
Switch Voltage Stress	High	High	Low	Low	High	High	High	High	High	Low
Switch Current Stress	Low	High	High	High	High	High	Low	High	High	High
Input Ripple	Low	Low	Low	Low	Low	Low	Low	High	Low	Low
Output Ripple	Low	Low	Low	Low	Low	Low	Low	Low	Low	Low
Switching devices conduction in T_s	4	2	2	3	3	2	3	1	3	1
Mode of Operation	CCM	DCM	DCM	DCM	DCM	DCM	DCM	DCM	DCM	DCM
Sensor	4	1	1	1	1	1	1	1	1	1

3.8. Loss Analysis

This section provides the loss equations required for the calculation of losses in different components of the power converter.

3.8.1 Semiconductor losses

There are two types of losses in the power semiconductor devices; (1) conduction losses and (2) switching losses.

Conduction losses: The loss occurring because of the ON resistance of the SiC switches (MOSFETs) is the conduction loss. Total conduction loss '$P_{switch,c}$' of the proposed converter contributed by MOSFETs.

$$P_{switch,c} = 2\, i^2_{sw,rms}\, R_{ds,on} \tag{3.32}$$

where '$R_{ds,on}$' is the on-state resistance of the MOSFET and '$i_{sw,rms}$' is the switch RMS current. Similarly, the diodes conduction losses are calculated using the values of on-state resistance, 'R_D' and the forward voltage drop, 'V_f'. The total conduction loss '$P_{diode,c}$' in the diodes.

$$P_{diode,c} = 2\, (i^2_{D,rms}\, R_D + i_{D,avg}\, V_f) \tag{3.33}$$

where '$i_{D,rms}$' and '$i_{D,avg}$' are the RMS and average current through the diode, respectively. Therefore, total conduction loss 'P_{cond}' is given by

$$P_{cond} = P_{switch,c} + P_{diode,c} \tag{3.34}$$

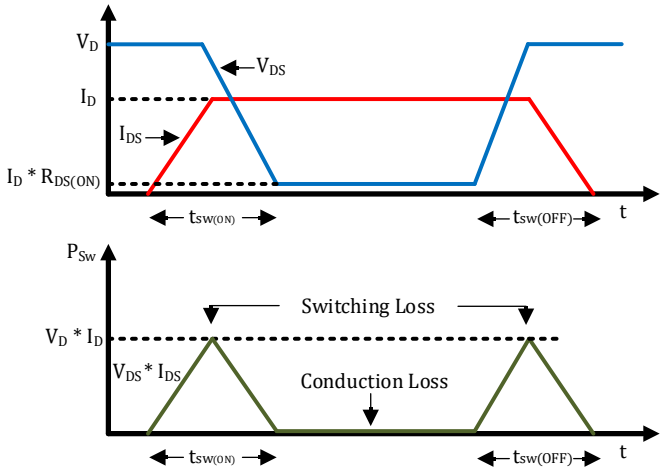

Fig. 3.17. Overlapping switch voltage and current during turn ON and turn OFF

Switching loss:

The switching losses are categorised into three parts. The first part is because of voltage and current overlapping during the turn on '$P_{switch,ON}$' and turn off '$P_{switch,OFF}$' of the SiC MOSFET as shown in fig. 3.17 [60]. The parasitic capacitance charging and discharging is also responsible for the switching losses which is the second part. And the gate drive loss is the third part.

Turn on loss:

$$P_{switch,ON} = \frac{1}{2} I_{sw,avg} V_{sw,avg} t_{on} f_{sw} \tag{3.35}$$

Turn off loss:

$$P_{switch,OFF} = \frac{1}{2} I_{sw,avg} V_{sw,avg} t_{off} f_{sw} \tag{3.36}$$

where '$I_{sw,avg}$', '$V_{sw,avg}$', and 'f_{sw}' are the average switch current, average switch voltage, and switching frequency, respectively. 't_{on}' and 't_{off}' are the overlapping period during MOSFET turn ON and turn OFF.

Switch Output Capacitance Loss:

The switch output capacitance loss 'P_{cap}' due to charging and discharging is given as

$$P_{cap} = 2 \left(\frac{C_{oss} f_{sw}}{2\pi} \int_0^{2\pi} V_{sw}^2(\omega t)\, d\omega t \right) \tag{3.37}$$

where 'C_{oss}' stands for switch output capacitance.

Gate Drive Loss:

The gate drive loss '$P_{sw,G}$' is derived as

$$P_{sw,G} = 2\, C_{iss}\, V_g^2\, f_{sw} \tag{3.38}$$

where 'C_{iss}' is the MOSFET input capacitance. The total switching loss is given as

$$P_{sw} = P_{switch,on} + P_{switch,off} + P_{cap} + P_{sw,G} \tag{3.39}$$

Therefore, the total semiconductor loss is

$$P_{sem} = P_{sw} + P_{cond} \tag{3.40}$$

3.8.2 Inductor losses

There are two inductors in the proposed converter. The losses for the input and the output

inductors are calculated as follows.

Input Inductor:

The input inductor losses '$P_{L,in}$' are due to AC resistance, 'R_{ac}'

$$P_{L,in} = I^2_{L,in\ rms}\, R_{ac} \tag{3.41}$$

where '$I_{L,in\ rms}$' is the input inductor RMS current.

Output Inductor:

The output inductor loss '$P_{L,out}$' is

$$P_{L,out} = I^2_{L,out\ rms}\, R_{ac} \tag{3.42}$$

where '$I_{L,out\ rms}$' is the output inductor output current.

Core loss:

Core loss 'P_{core}' of the inductors can be calculated as

$$P_{core} = P_{c,l}\, V_e \tag{3.43}$$

where '$P_{c,l}$' and 'V_e' are the inductor core loss limit and effective core volume, respectively.

3.8.3 Capacitor loss

The transfer capacitor 'C_t' and the output capacitor losses '$P_{l,cap}$' can be calculated as

$$P_{l,cap} = I^2_{rms}\, R_{ESR} \tag{3.44}$$

where 'I_{rms}' is the RMS current through capacitor and 'R_{ESR}' is the equivalent series resistance.

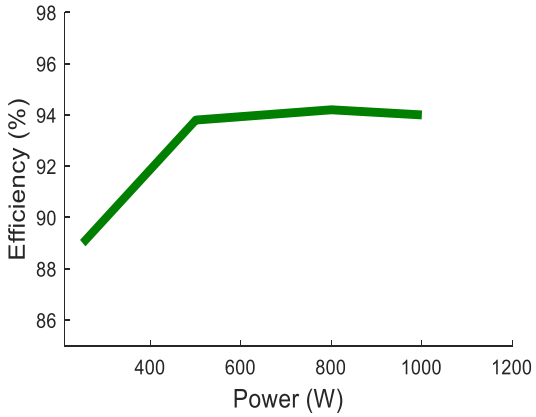

Fig. 3.18. Efficiency curve

Table 3.6: Parameter Values for Loss Analysis

Parameter	Value
$R_{ds,ON}$	27 mΩ
R_D	4.6 mΩ
V_f	1.2 V
C_{oss}	320 pF
C_{iss}	1500 pF
$R_{ac,i}$	79.45 mΩ
$R_{ac,o}$	17.66 mΩ
$P_{c,l}$	44000 mm^3
V_e	22000 W/set
$R_{ESR,f}$	35.63 mΩ
$R_{ESR,e}$	182.23 mΩ

The loss analysis is done utilizing the equations in [61] and by using information provided in components' datasheet, which are listed in Table 3.6. The light-load and full-load efficiency of the proposed converter are 89% and 94%, respectively. The efficiency over the entire load is shown in fig. 3.18. Table 3.7 lists the complete breakdown of the power losses in the converter design at output power of 1 kW.

Table 3.7: Breakdown of Losses for Rated Output Power

Device	Power loss (W)
Power switch	19.10
Diode	6.70
Transfer capacitor	1.00
Output capacitor	8.35
Input inductor	5.60
Output inductor	11.00
Constant losses	12.00
Total power loss	63.75
Efficiency	94%

Fig. 3.19 shows the pie chart representation of the same power loss to make it easier to identify the loss share among different components of the converter. The maximum power loss is due to the MOSFETs, which is usual.

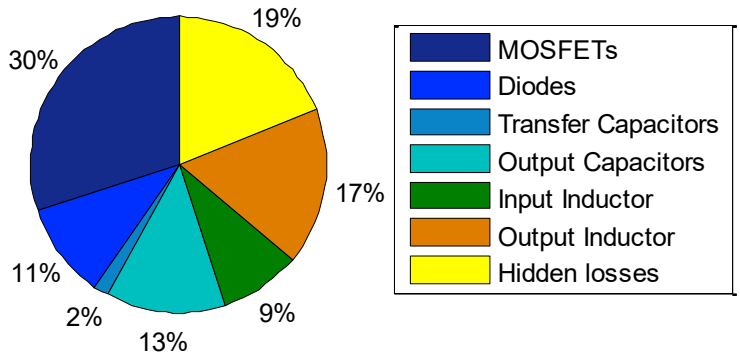

Fig. 3.19. Pie chart representing percentage loss in different components

Fig. 3.20 shows the efficiency comparison of different topologies with the proposed converter. The experiment shows that the measured and calculated efficiencies are nearly equal.

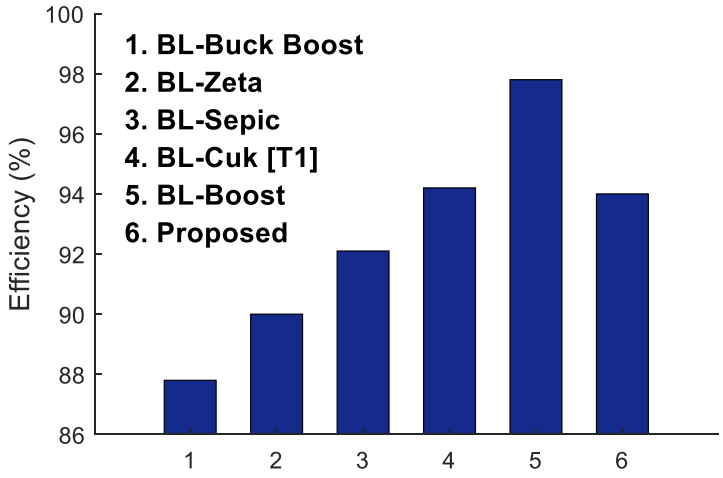

Fig. 3.20. Bar graph representing efficiency comparison

3.9. Conclusion

A novel single-sensor based bridgeless Cuk-derived PFC converter with reduced components' count for on-board G2V charging is presented. The proposed converter output inductor is designed to operate in DCM for the complete power range to attain PFC naturally at the AC supply, and as a result the sensor requirement reduces which decreases the cost, and enhances robustness of the converter towards high-frequency noise. The devices in the proposed bridgeless Cuk-derived converter has lower voltage stress as compared to the traditional Cuk PFC converter, which results in reduced switching losses and enhancement of the overall converter

efficiency. Further, throughout the converter operating range only a single semiconductor device is in current conduction path, thus, reducing the converter conduction losses, and making the thermal management simple. This chapter provides a brief discussion on different bridgeless Cuk-derived topologies. The converter detailed steady-state analysis over one switching cycle is presented along with the design. The detailed small-signal-modeling and the closed loop controller design for novel Cuk-based PFC converter for onboard EV charger are presented. The control-to-output transfer function of the Cuk-based converter is derived. A systematic procedure to design the voltage loop is provided. The converter analysis and the design are validated through simulation results using PSIM 11. A proof-of-concept hardware prototype rated at 1 kW has been tested to confirm the converter high performance. THD of 3.49 % and a PF of 0.9994 are achieved at full load in the hardware prototype. The work also provides a detailed attributes comparison chart with state-of-the-art bridgeless topologies. Extensive loss analysis of the proposed converter at full load condition is done. High efficiency of 94% is achieved in the hardware prototype and additionally, the efficiency has been compared with different prevailing topologies.

CHAPTER 4: SINGLE PHASE BRIDGELESS CUK DERIVED DC-DC CONVERTER FOR VEHICLE TO VEHICLE CHARGE TRANSFER

4.1. Introduction

Widespread electric vehicle (EV) adoption is critically challenged by the limited range of driving, longer charging duration, and non-availability of charging stations everywhere [62]. The flexibility of the EVs can be enhanced using the vehicle-to-vehicle (V2V) charging system. This system will help in mitigating the range anxiety and also offers emergency charge transfer to another user.

According to a report released by Idaho National Laboratory (INL) [63], about 85 % EV owners recharge the EV batteries at their residence. The main reason behind this is the non-availability of battery charging stations at different locations at present as well as cost. Development of new charging stations involves extra cost and the EVs are limited to locations close to grid infrastructure.

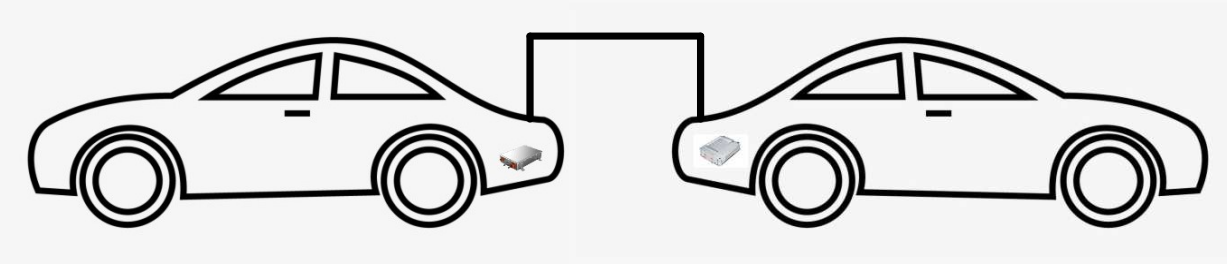

Fig 4.1. Vehicle-to-Vehicle (V2V) Charging using On-board EV Charger

The energy exchange between EVs can be a viable option in an emergency situation where an EV is about to run out of charge at a location without any charging station nearby, then another EV with enough state-of-charge can transfer the energy required by the first EV. The V2V charging operation is represented in Fig. 4.1. Different EV charging techniques have been reported in literature [64]-[71]. However, very few investigations from power electronics perspective on the domain of V2V charging have been reported. This Chapter presents the V2V charging functionality as shown in Fig 4.2 of an EV.

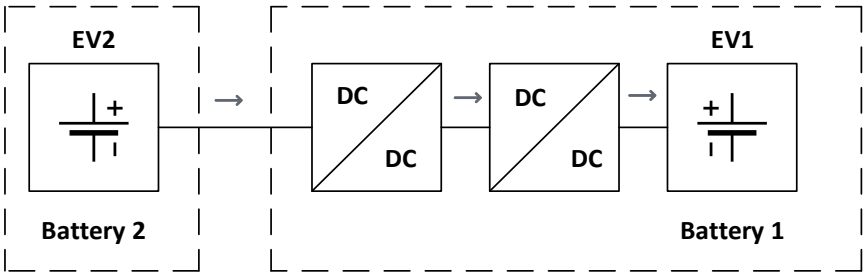

Fig 4.2. Proposed V2V Charging Configuration using On-board EV Charger

4.2. Different Vehicle to Vehicle Charging Techniques

This section describes the various charging modes for the V2V power transfer between two EVs [72]-[78].

4.2.1. V2V Power Transfer in AC Mode

The power transfer in AC mode for the V2V charging operation are described below:

(I) Indirect Traditional Approach: In this method, the power grid is used as an intermediate point. Here the V2G operation is combined with G2V

(II) Direct Approach: In this method, the connection to the power grid is not necessary. Here the V2H operation is combined with the G2V operation.

The power transfer takes place between two EVs where EV1 is transmitting power to EV2 in all the considered cases. The battery charger in each of the EV comprises front end AC-DC converter and a back-end DC-DC converter for implementing the V2G and G2V operations, the converters are bidirectional.

4.2.1.1. V2G Operation in Combination with G2V Operation

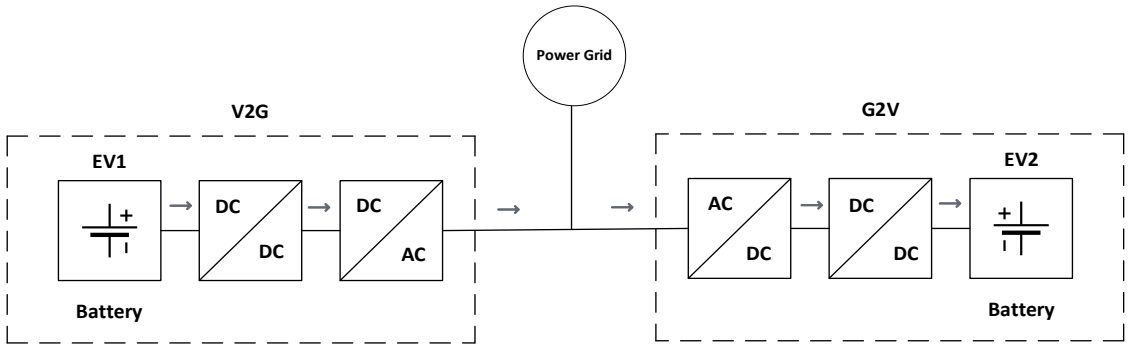

Fig 4.3. V2G Operation in Combination with G2V Operation

This method combines the two operational modes of V2G and G2V where both the EVs have a connection to the power grid, which is presented in Fig. 4.3. EV1 is providing the energy and is operating in V2G mode where it injects the stored energy into the batteries to the power grid. EV2 works in G2V mode and recharges the batteries by accepting energy from the grid. The two EVs are in connection with the power grid. The flow of power is controlled by current regulation on the AC side. The current between two EVs has 180 degrees phase-shift. The resultant current of the power grid is zero as the current requirement of EV2 is equal in amplitude to the current generated by EV1 or a set of EVs. The physical meaning is that the energy requirement for recharging EV2 batteries is completely furnished by EV1. Therefore, the power grid does not get overloaded, which represents the critical aspect of V2V operation.

4.2.1.2. V2H Operation in Combination with G2V Operation

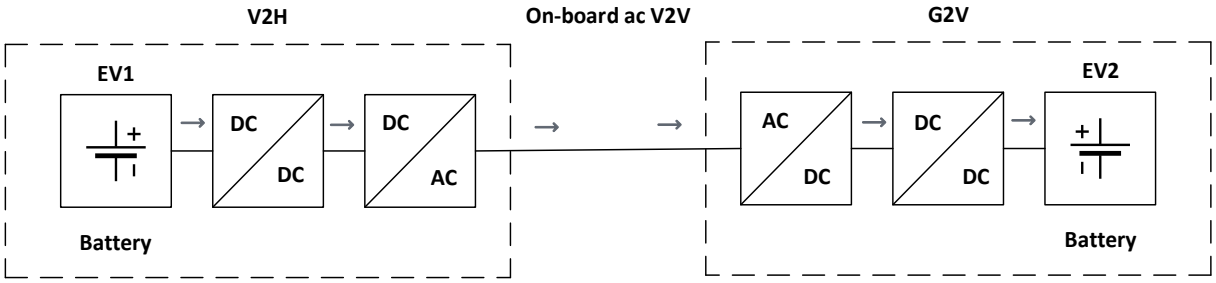

Fig 4.4. V2H Operation in Combination with G2V Operation

On the contrary to the previous case, there is a possibility of direct V2V transfer of power utilizing AC power. The V2H mode of operation is an aspect of isolated systems in which there is no connection to the power grid. In this case, an EV is regulated to generate AC voltage to give energy to the electrical loads. The method can be utilized for V2V power transfer where EV1 acts as the AC voltage source work in V2H mode as depicted in Fig 4.4 and the EV is feeding from it working in G2V mode where the current and voltage are in-phase. The difference between the traditional and direct method is that in the latter there is no power grid connection. As there is no grid connection in the second method, it is considered as direct method because the two EVs are only connected to each other and there is a direct V2V power transfer between them. This approach is a good option when the batteries of the EVs are completely discharged and there is no possibility to move.

4.2.2. V2V Power Transfer in DC Mode

This section describes the methods of DC mode V2V power transfer. There are several advantages to the direct V2V power transfer in AC mode, which combines the V2H and G2V modes. But there are four power conversion stages in AC V2V power transfer irrespective of direct or traditional method. As the batteries are charged using DC power, there is an advantage in connecting the EVs using the DC terminals. This can be implemented using the following methods:

(i) On-board DC-DC converter: In this method, both the EVs will have on-board DC-DC converter and the power will be transferred by establishing a back-to-back connection between them.

(ii) Off-board DC-DC converter: In this method, an external DC-DC converter is used to connect the battery terminals in both the EVs.

4.2.2.1. V2V Charging using On-board DC-DC Converter

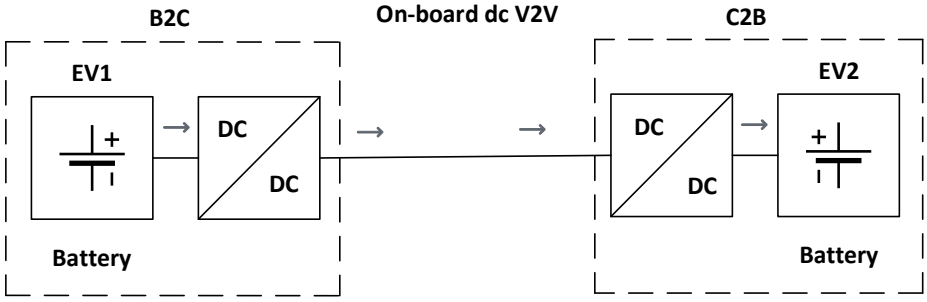

Fig 4.5. V2V Charging using On-board DC-DC Converter

A bidirectional power flow is allowed in the on-board EV battery charger so that the V2G and G2V operations can be implemented. Therefore, the DC-DC converter for the battery chargers permits the batteries to be charged and discharged with current or voltage control. Suppose a second DC-DC converter is joined at the output of the first DC-DC converter and both the dc-dc converter can operate in bidirectional mode then a power exchange is possible between the two EVs batteries. This is outlined in Fig. 4.5. The cascaded DC-DC converter permits bidirectional operation with a regulated charging current in a varied operating voltage range. There is a possibility to charge batteries having higher voltage using lower voltage batteries.

The EV connections should be using the DC links for such condition. The DC link nodes are common to both the DC-DC and AC-DC converters for each charger. Thus, the external plug that is connected to enable the V2V power transfer in DC mode do not require any additional power converters or hardware.

4.2.2.2 V2V Charging using Off-board DC-DC Converter

The V2V power transfer is possible using an off-board DC-DC converter instead of an on-board charger. This is a useful method when there is a need of galvanic isolation or in situations when there is a significant voltage difference in EV batteries. In such cases, the EVs should be interfaced directly to the batteries and is shown in Fig. 4.6. The on-board battery charger operation is not required in such a case because as the off-board DC-DC converters permit the operation using regulated current or voltage. An off-board charger does not require a power source as each of the terminals are connected to the batteries of each EV. Thus, to enable this mode of operation, the power plug must comprise of power semiconductors and high frequency transformer. Though there is no requirement to use the on-board EV chargers, which is an advantage to the EVs but the external DC-DC converter for off-board V2V EV charging comprises extra cost in comparison to the on-board charging solution. Therefore, this Chapter presents a novel V2V charge transfer using the proposed converter where only the on-board charger of the EV to be charged is utilized for charging the EV battery.

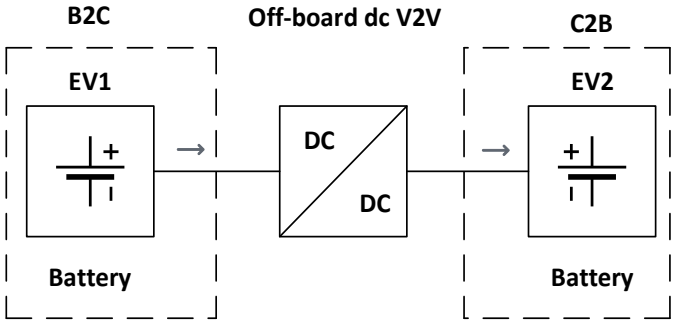

Fig 4.6. V2V Charging using Offboard DC-DC Converter

4.3. Proposed Converter Working Conception in DC Charging Mode

The proposed single-phase Cuk-derived bridgeless converter in V2V DC charging mode is presented in Fig. 4.7. The basic set-up of the converter incorporates a bidirectional switch, two diodes at the output, two inductors, one at the input and the other at the output, and three capacitors,

which comprises of one transfer capacitor and two output capacitors. The bidirectional switch is connected by joining two MOSFETs back-to-back, which are driven using the same PWM signal. Therefore, it is counted as one. The special feature of the converter is the reduced components' count, which is two less than the conventional Cuk converter. Diode 'D_{o2}' conducts when the switch is ON and diode 'D_{o1}' conducts when the switch is OFF. The switch voltage stress and diode voltage stress of the converter in DC charging mode is ($V_o - \frac{V_{in}}{2}$) and V_o, respectively, which is an added advantage as the voltage stress in conventional Cuk converter is ($V_{in} + V_o$). Therefore, the efficiency of the converter increases as the switching losses are reduced.

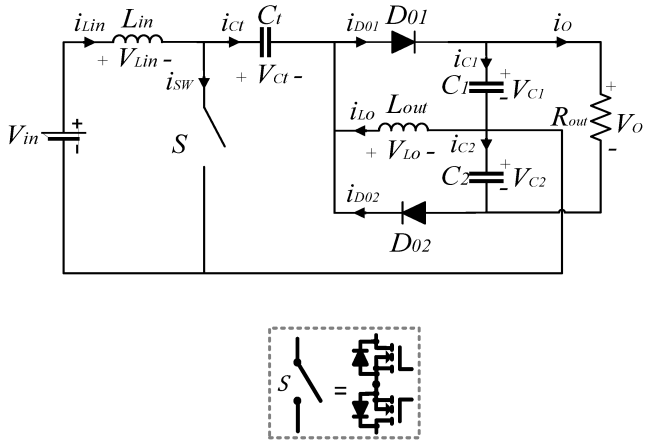

Fig. 4.7. The proposed single-phase bridgeless Cuk-derived DC-DC converter

4.4. Steady State Analysis

The steady-state analysis of the proposed converter in DC charging mode is presented in this section. The analysis for one switching cycle is discussed here and the crucial waveforms are described in Fig 4.8. Four operating modes are observed during one switching cycle. The equivalent circuits of all four modes of operation are shown in Fig. 4.9.

The following assumptions are made for the analysis of the converter:

a) All components are considered ideal and lossless.
b) The transfer capacitor 'C_t' average voltage equal to input voltage.
c) The input and output voltage are considered to be constant during one switching cycle.
d) The filter capacitors at the output are large enough so that the output voltage is constant during one switching cycle.

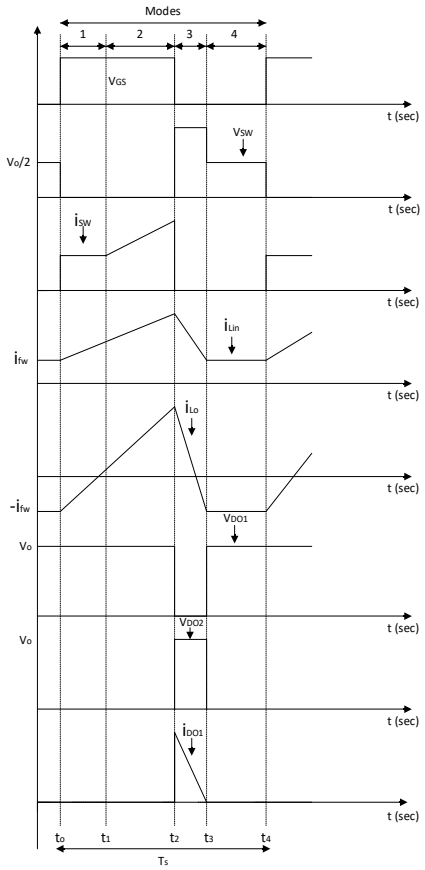

Fig. 4.8. The proposed BL-Cuk derived DC-DC converter waveforms for one switching cycle

DC-DC Converter Operation Description:

Mode 1 ($t_o - t_1$): The switch 'S' and diode 'D_{o2}'are conducting in this mode. Before entering this mode, the input current 'i_{Lin}' freewheels in the loop, which is formed by 'V_{in}' 'L_{in}' 'C_t' and 'L_o'. The freewheeling current is shown as 'i_{fw}'. The equivalent circuit of the converter is shown in Fig 4.9(a). The input inductor 'L_{in}' and output inductor 'L_o' store energy from the battery source 'V_{in}' and the transfer capacitor 'C_t' having a slope of $\frac{V_{in}}{L_{in}}$ and $\frac{V_{in}}{L_o}$, respectively.

$$i_{Lin} = i_{fw} + \frac{V_{in}}{L_{in}}t \tag{4.1}$$

$$i_{Lo} = -i_{fw} + \frac{V_{in}}{L_o}t \tag{4.2}$$

Mode 2 ($t_1 - t_2$): The switch 'S' is conducting and all the output diodes are in blocking mode. In this mode, the input inductor 'L_{in}' and output inductor 'L_o' continues to store energy from the battery and transfer capacitor, respectively. The equivalent circuit is shown in Fig 4.9(b).

$$i_{Lin} = i_{fw} + \frac{2V_{in}}{L_{in}}t \tag{4.3}$$

$$i_{Lo} = -i_{fw} + \frac{2V_{in}}{L_o}t \tag{4.4}$$

Mode 3 ($t_2 - t_3$): The switch S is turned off and the diode 'D_{o1}' is conducting in this mode. The input inductor current 'i_{Lin}' and the output inductor current 'i_{Lo}' has reached their peak values before entering this mode. The input and output inductor are demagnetizing to the load while the output capacitor 'C_1' and transfer capacitor 'C_t' are getting charged. The equivalent circuit is shown in Fig 4.9(c).

$$i_{Lin} = i_{fw} + \frac{2V_{in}}{L_{in}}DT_s - \frac{7V_o}{8L_{in}}t \tag{4.5}$$

$$i_{Lo} = -i_{fw} + \frac{2V_{in}}{L_o}DT_s - \frac{7V_o}{8L_o}t \tag{4.6}$$

where $DT_s = T_{on}$ which is the ON time of the switch. The mode ends when 'I_{Do1}' becomes zero. Therefore,

$$i_{Lin} + i_{Lo} = 0 \tag{4.7}$$

Solving (4.7), we derive

$$D_1T_s = \frac{16V_{in}}{7V_o}DT_s \tag{4.8}$$

where D_1T_s is the time duration of mode 3.

Mode 4 ($t_3 - t_4$): In this mode, the load supplied by the output capacitors 'C_1' and 'C_2' as all the output diodes and the bidirectional switch are in OFF state. The equivalent circuit of this mode is shown in Fig 4.9(d).

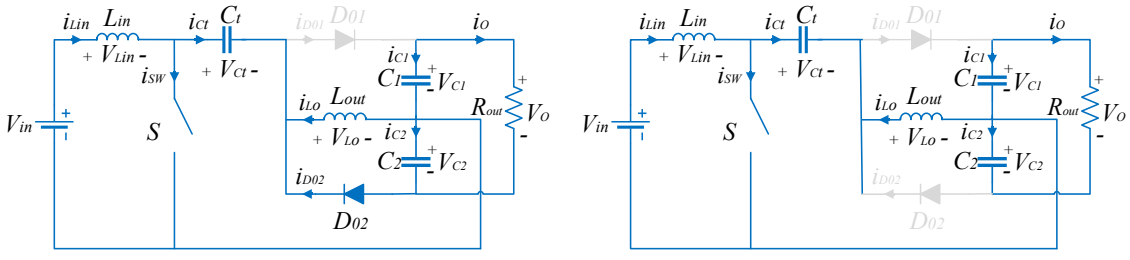

(a) (b)

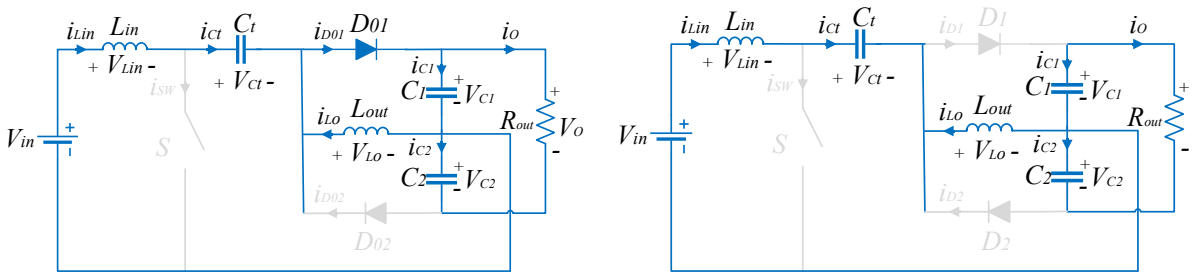

Fig. 4.9. Proposed BL-Cuk DC-DC converter equivalent circuits; (a) Mode-1; (b) Mode-2; (c) Mode-3; (d) Mode-4.

4.5. Converter Design

The following section provides the detailed design procedure of the bridgeless Cuk-derived DC-DC converter for V2V charging operation.

4.5.1. Condition for Discontinuous Current Operation

The condition to ensure discontinuous current operation of the converter is

$$DT_s + D_1T_s \leq T_s \tag{4.9}$$

$$D + D_1 \leq 1 \tag{4.10}$$

$$D \leq \frac{7M}{7M+16} \tag{4.11}$$

where $M = \frac{V_o}{V_{in}}$. From (4.11), for a given duty cycle the critical voltage conversion ratio 'M_{cr}' can be obtained as

$$M_{cr} \geq \frac{2D}{1-D} \tag{4.12}$$

To operate the converter as per requirement, the converter voltage gain must be

$$M \geq M_{cr} \geq 8 \tag{4.13}$$

4.5.2. Average Output Current

The converter output current in DC charging mode is equal to the average current value of the output diode current 'I_{DO1}'. The average diode current can be found using the following expression as the output diode 'D_{o1}' current is triangular in shape.

$$i_{Do1,avg} = \frac{i_{Do1,pk} D_1 T_s}{2T_s} \tag{4.14}$$

where the value of $i_{Do1,pk} = \frac{V_{in}}{L_{eq}} DT_s$ is the maximum value of the output diode 'D_{o1}' current and the value of $L_{eq} = \frac{L_{in} L_o}{L_{in} + L_o}$. Solving (4.14),

$$i_{Do1,avg} = \frac{8 V_{in}^2 D^2 T_s}{7 L_{eq} V_o} \tag{4.15}$$

Now integrating (4.15) for half line period, the power converter average output current in DC charging mode for a line period is derived and is given in (4.16).

$$I_{Do1,avg} = \frac{4 V_{in}^2 D^2 T_s}{7\, L_{eq} V_o} \tag{4.16}$$

4.5.3. Passive Components Design of Converter

The design of input inductor is in terms of the input current ripple allowed in a switching cycle and 'Δi_{Lin}' is given by

$$\Delta i_{Lin} = \frac{V_{pk}}{L_{in}} DT_s \tag{4.17}$$

$$L_{in} = \frac{V_{pk}}{\Delta i_{Lin}} DT_s \tag{4.18}$$

The value of output inductor 'L_o' is given by

$$L_o = \frac{L_{in} L_{eq}}{L_{in} - L_{eq}} \tag{4.19}$$

The value of 'L_{eq}' is obtained from (4.11) and (4.16) which is given as

$$L_{eq} \leq \frac{28 V_{in}^2 {V_o}^2 T_s}{P_{out}(7V_o + 16V_{in})^2} \tag{4.20}$$

Where P_{out} = power converter rated output power.

The output capacitor is designed considering $C_1 = C_2 = C_o$

$$\Delta V_{o,ripple} = \frac{1}{C_o} \left(\int i_{co_1} dt + \int i_{co_2} dt \right) \tag{4.21}$$

$$\Delta V_{o,ripple} = \frac{1}{C_o} \left(\int i_{D_{o1},avg} - 2i_o \right) dt \tag{4.22}$$

$$=\frac{2i_o}{\omega C_o} \tag{4.23}$$

$$C_o=\frac{2i_o}{\omega_{\Delta \mathrm{Vo,ripple}}} \tag{4.24}$$

The design of transfer capacitor 'C_t' in DC charging mode is designed similar to the AC charging mode which is given by

$$f_{res}=\frac{1}{2\pi\sqrt{C_t(L_{in}+L_o)}} \tag{4.25}$$

where f_{res} is defined as the resonant frequency.

4.6. Results and Discussions

The following section details the results and discussions about the simulation and hardware experimentation.

4.6.1. Simulation Results

PSIM 11 is used to model and simulate the proposed Cuk-derived converter as DC-DC converter . Table 4.1 and Table 4.2 details the input specifications and design parameters for the power converter simulation in DC charging mode, respectively. Fig 4.10(a) shows the DC input current and DC input voltage. The DC output voltage and current at rated output are demonstrated in Fig 4.10(b). It can be observed that the output voltage exactly settles at 400V.

Table 4.1: Input Specifications

Parameter	Value
Input Voltage (V_{in} (rms))	48 V
Output Voltage (V_o)	400 V
Output Power (P_o)	500 W
Input Current Ripple ($I_{in,\ ripple}$)	5%
Switching Frequency (f_{sw})	50kHz

The converter intermediate capacitor voltage and its average are shown in Fig 4.10(c), which validates that average voltage of the transfer capacitor is equal to source voltage. Fig 4.10(d) depicts the diodes voltage 'V_{Do1}' and 'V_{Do2}' having peak voltage stress of 400V, which is equal to the output voltage. Fig 4.10(e) shows the output diode current and its average, which is equal to output current thus, aligning with the analysis. The voltage across the two output capacitors are shown in Fig. 4.10 (f). C_{o1} is charging more as higher current flows through it whereas C_{o2} is

charging less due to lower current flow through it.

Table 4.2: Design Parameters

Parameter	Value
Maximum Duty Cycle (D_{max})	0.785
Input Inductor (L_{in})	1.5 mH
Output Inductor (L_o)	15 µH
Transfer Capacitor (C_t)	2.3 µF
Output Cpacitor (C_{o1}, C_{o2})	1.66 mF

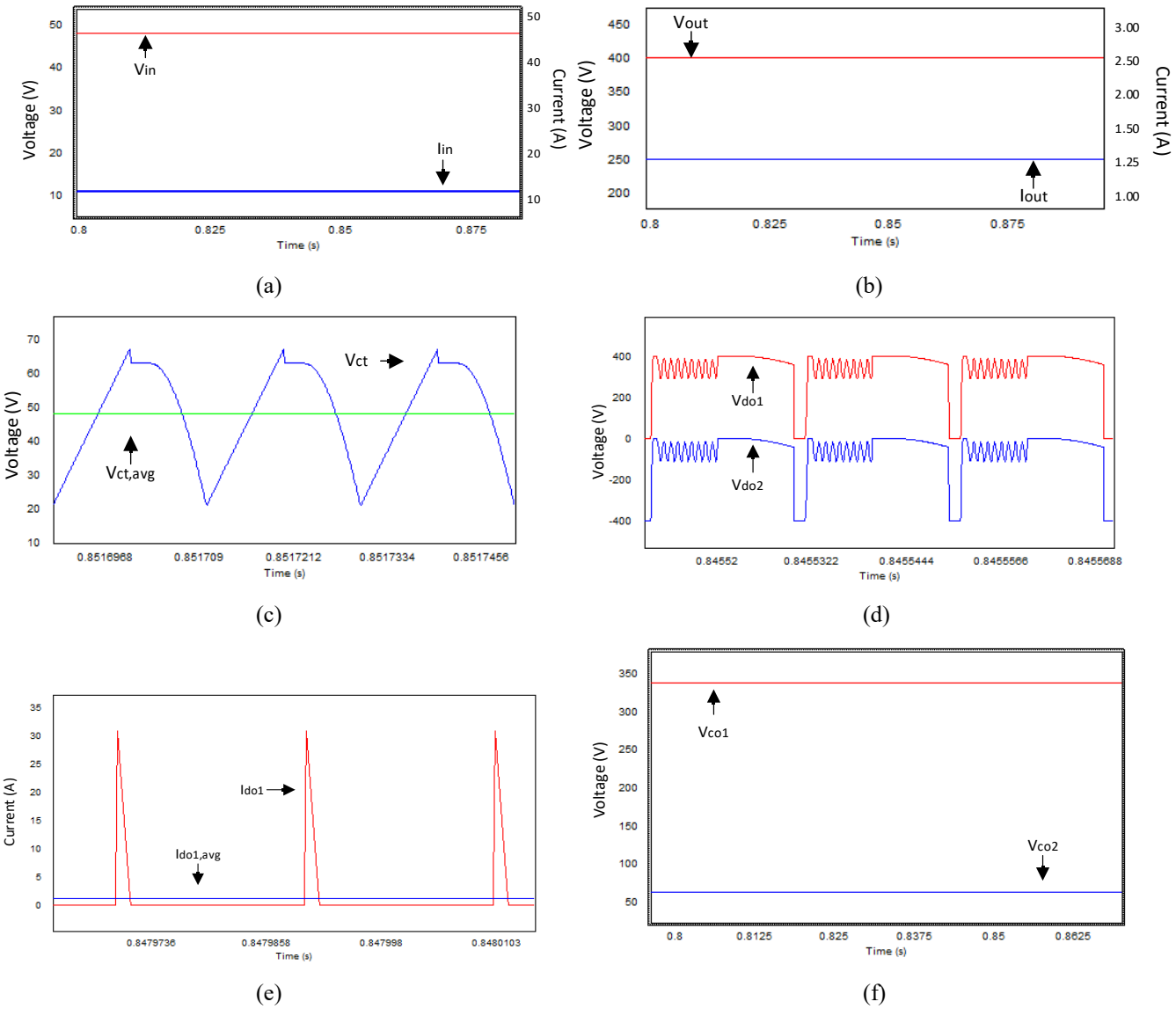

Fig. 4.10. Simulation results (a) Source dc voltage and source dc current; (b) output dc voltage and dc current; (c) Transfer capacitor voltage and its average; ; (d) diode 'D_{o1}' and diode 'D_{o2}' voltage; (e) output diode current and its average; (f) output capacitors voltage;

4.6.2. Experimental Results

A 500W hardware prototype is developed in the laboratory for validating the converter design in DC charging mode which is shown in Fig 4.11. Table 4.3 lists the components used to build the experimental hardware prototype. The gate signals of the power switch are generated by coding the TI-DSP-TMS320F28335. For designing the input inductor, the peak input current ripple of 5% is considered.

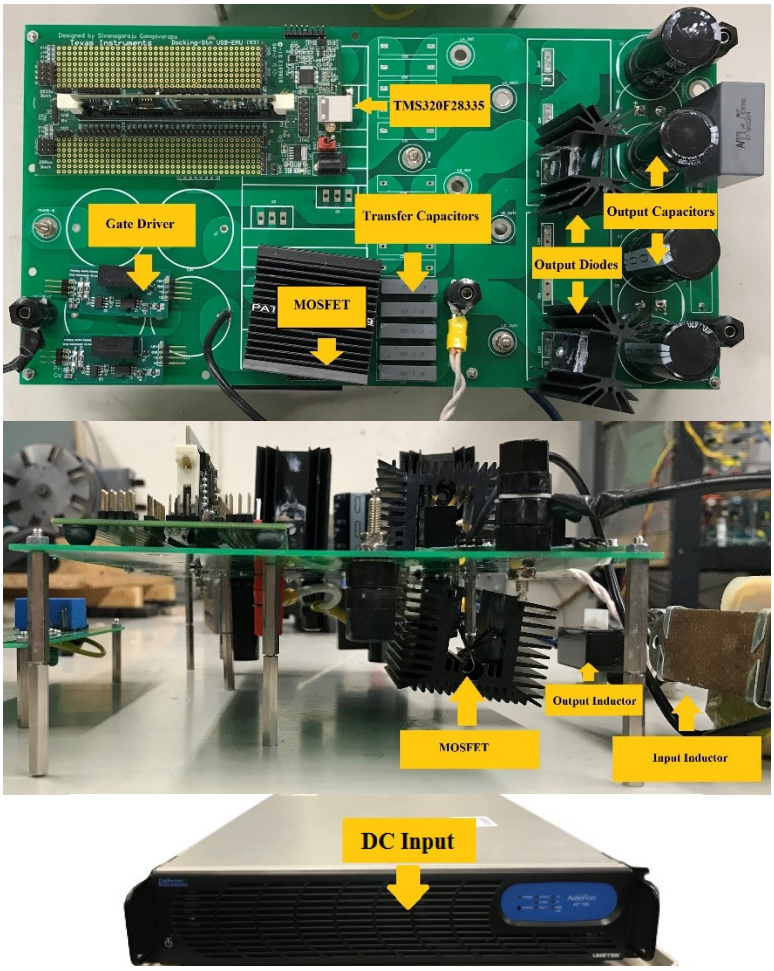

Fig. 4.11. Experimental hardware prototype setup of the proposed BL-Cuk DC-DC converter

The experimental steady-state output waveforms of the proposed converter in DC charging mode are shown in Fig 4.12. The DC input voltage and current along with the DC output voltage and current at 500W and 250W are shown in Fig. 4.12(a) and Fig. 4.12(b), respectively. The intermediate capacitor average voltage is equal to the input voltage, which is represented in Fig. 4.12(c) thus, making assumption (d) evident. Fig. 4.12(d) shows the zoomed output diode voltage,

which confirms that one diode is conducting and the other is in blocked mode having voltage stress of 400 V. The zoomed version of bidirectional switch voltage is shown in Fig. 4.12(e). The difference in switch voltage levels is due to difference in voltage levels of the output capacitors. Switch voltage along with the gate signal can be is seen in Fig. 4.12(f). Fig. 4.12(g) demonstrates the output diode current. Fig. 4.12(h) shows the output capacitors voltage along with output DC voltage. The voltage levels are different due to difference in capacitor current. A high efficiency of 95% is achieved in the proof-of-concept hardware prototype experimentation.

Table 4.3: Experimental Hardware Prototype Components Details

Component	Details
MOSFET	UJ3CO65030K3S, SiC
Diodes	60EPF12
Input Inductor (Lin)	159ZL-C14H
Output Inductor (L_O)	Ferrite core
Transfer Capacitors (C_t)	R71PI34704030M
Output Capacitors (C_{O1}, C_{o2})	ESMQ401VSN471MQ50W
DSP	TMS320F28335
Gate Driver	IC- IXYS-IXDN609SI
Power Source	California Instruments AST1503

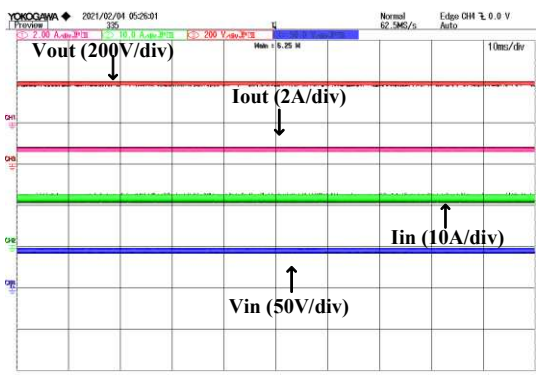

(a)

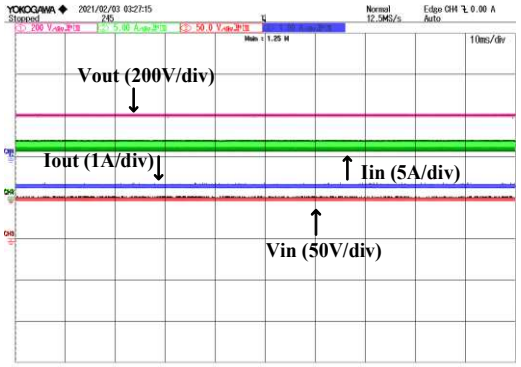

(b)

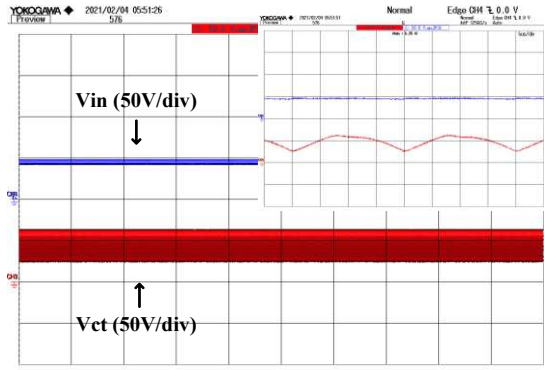

(c)

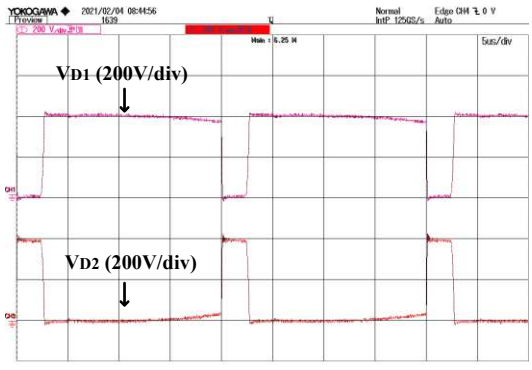

(d)

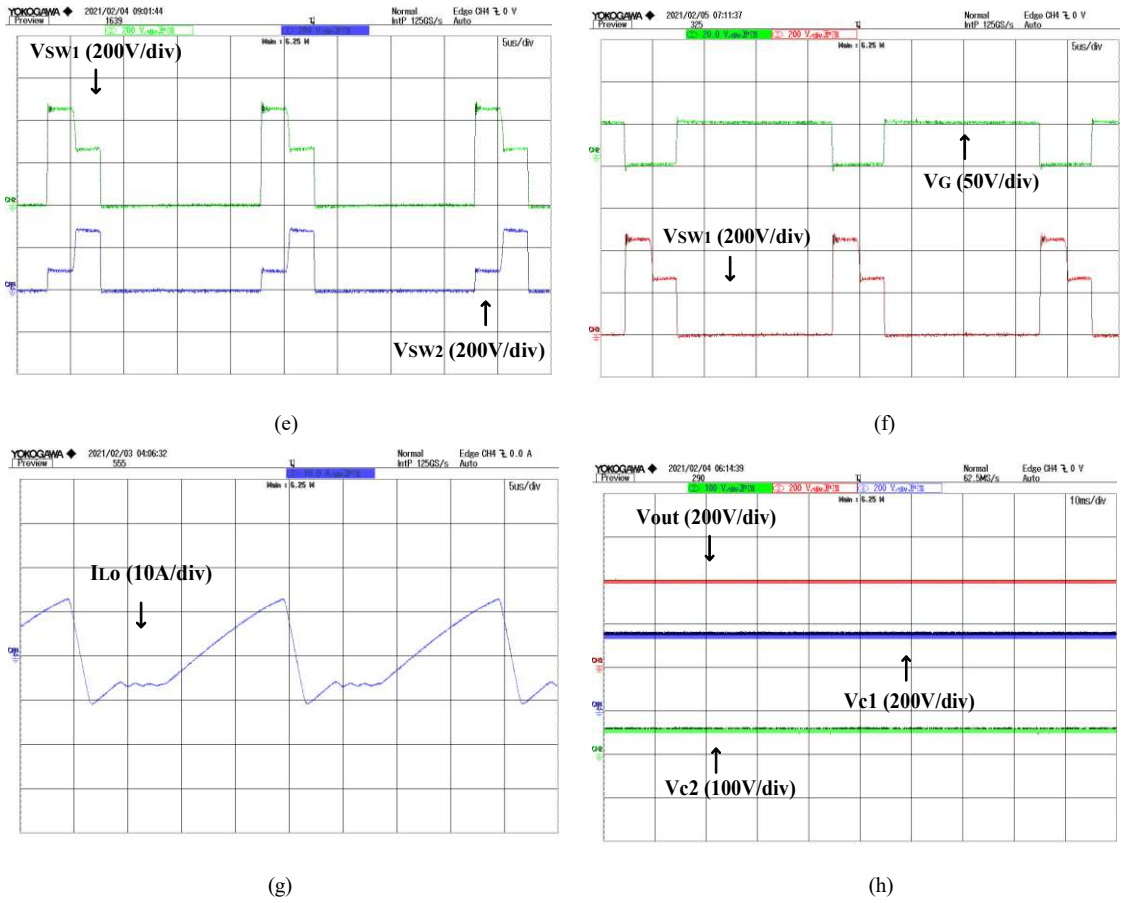

Fig. 4.12. Experimental results (a) DC input voltage and current with dc output voltage and output current at 500W; (b) DC input voltage and current with dc output voltage and output current at 250W; (c) Voltage across intermediate capacitor and input voltage; (d) Diode 'D_{o1}' and 'D_{o2}' voltage; (e) Bidirectional switch voltage; (f) Gate source voltage and switch voltage; (g) Output inductor current; (h) Output capacitor voltage and output voltage;

4.7. Efficiency Analysis

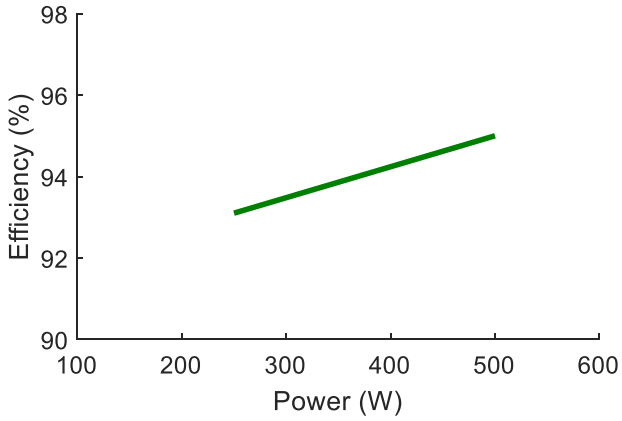

Fig. 4.13. Experimental hardware prototype measured efficiency curve

Table 4.4: Loss Equations

Description	Equations
MOSFET conduction loss	$i^2_{sw,rms} R_{ds,on}$
MOSFET switching loss	$\frac{1}{2} I_{sw,avg} V_{sw,avg} t_{off} f_{sw}$
Gate drive loss	$C_{iss} V_g^2 f_{sw}$
Total diode loss	$(i^2_{D,rms} R_D + i_{D,avg} V_f)$
Inductor loss	$I^2_{L,in\ rms} R_{dc}$
Capacitor loss	$I^2_{rms} R_{ESR}$

The experimental efficiency measured has been plotted in Fig 4.13 with respect to load variation. The loss occurring in the power converter has been analysed using the equations [79][80] listed in Table 4.4 as well as with the values obtained from the datasheet.

Table 4.5: Breakdown of Losses

Device	Power loss (W)
Power switch	14.20
Diode	3.00
Transfer capacitor	0.41
Output capacitor	1.43
Input inductor	4.82
Output inductor	0.62
Constant losses	0.32
Total power loss	24.80
Efficiency	95%

Table 4.5 lists the calculated values of the power losses occurring in various devices used in the proposed DC-DC converter at rated power of 500W and the theoretical efficiency is estimated from the same. Fig. 4.14 illustrates the pie chart presentation of the power loss breakdown to show the percentage of loss occurring in various components of the converter.

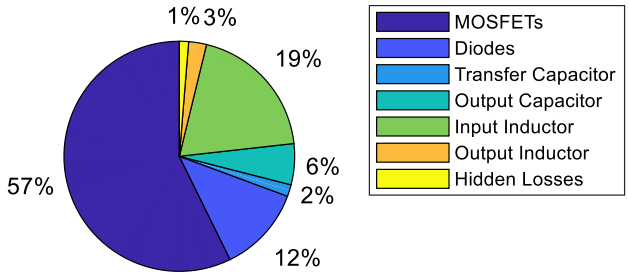

Fig. 4.14. Pie chart representing percentage loss in different components

MOSFETs contribute to the major power loss occurring in the converter which is 57% of the total loss. The diodes losses are 12% of the total loss. The losses in the semiconductor devices sum up to 69% of total loss. The rest 31% loss mainly come from the passive components. The input inductor contributes to the second highest power loss in the power converter. The efficiency measured from the proof-of-concept hardware and the analytically efficiency calculated are nearly equal.

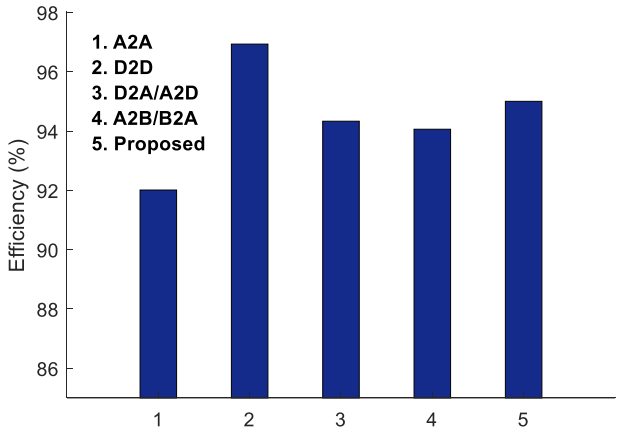

Fig. 4.15. Bar graph comparison of different V2V configuration efficiencies

The efficiency of the proposed configuration for V2V charging has been compared with different configurations reported in the literature [72] such as the ac-to-ac (A2A) interface, dc-to-dc (D2D) interface, dc-to-ac and ac-to-dc (D2A/A2D) interface, ac-to-battery and battery-to-ac (A2B/B2A) interface and the comparison has been represented in Fig 4.15. The efficiency data is further listed in numerical value in the Table 4.6.

Table 4.6: Efficiency Data

Mode	**Efficiency**
A2A	92.01 %
D2D	96.93 %
D2A/A2D	94.33 %
A2B/B2A	94.06 %
Proposed	95 %

4.8. Comparative Analysis

This section provides a comparative analysis of different state-of-art techniques [72] with the proposed technique used for V2V power transfer. Table 4.7 lists the important advantages and disadvantages of the proposed as well as various techniques reported in the literature. Fig. 4.16 represents the various configurations used for the comparative analysis.

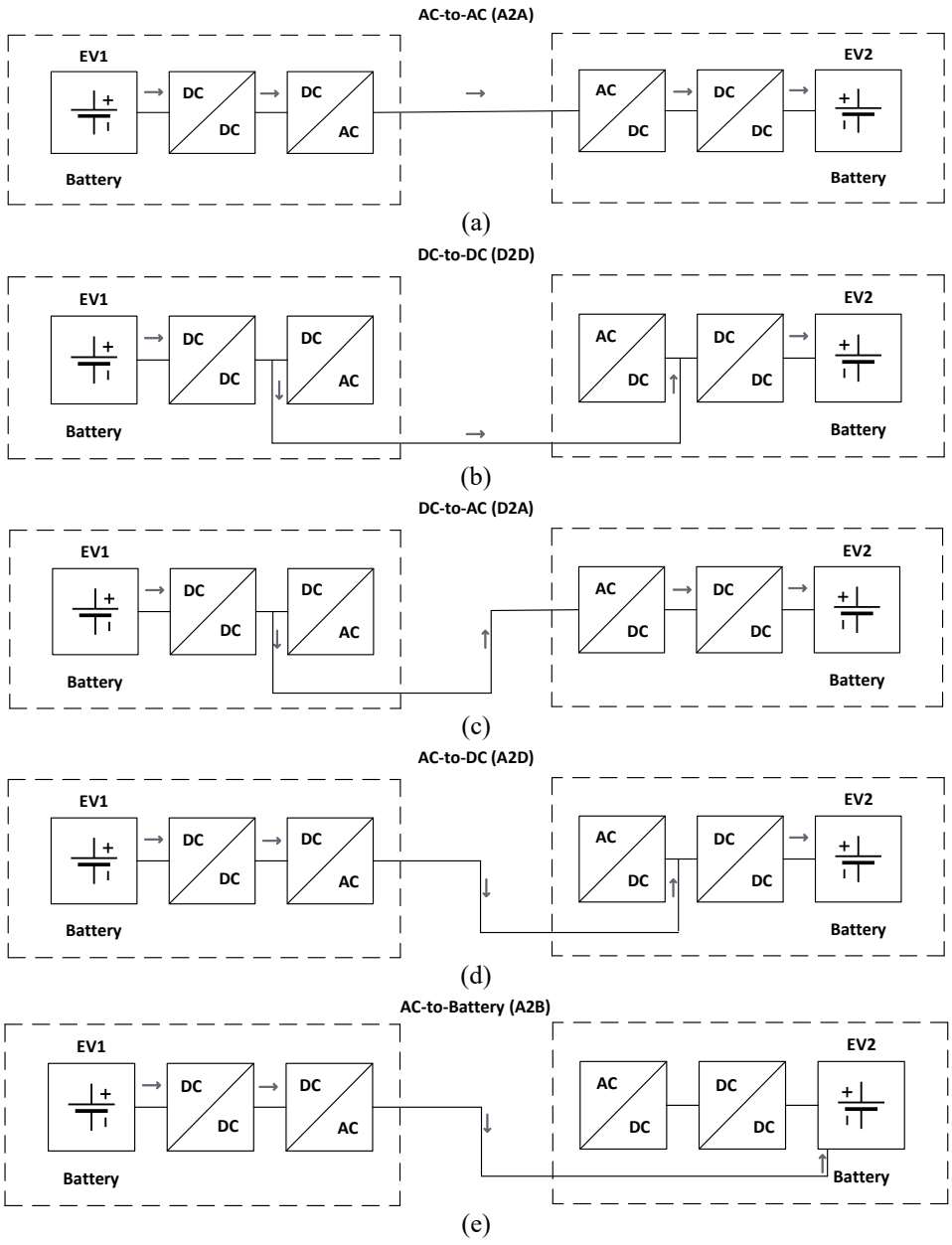

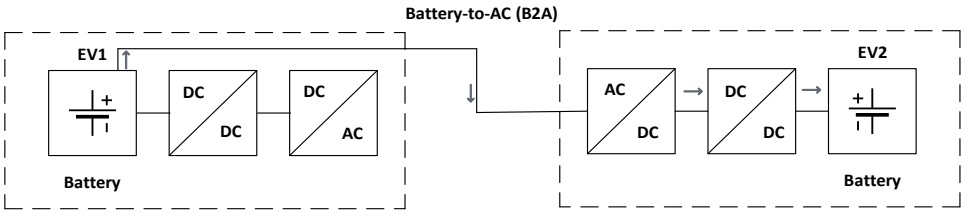

(f)

Fig. 4.16. V2V power transfer configurations: (a) A2A; (b) D2D; (c) D2A; (d) A2D; (e) A2B; (f) B2A;

Table 4.7: Comparative Analysis

Mode	Advantages	Disadvantages
A2A	• The already available terminals are used • Inrush current protection is available	• Redundant power conversion • Low efficiency
D2D	• Four quadrant operation is possible • Eliminated two redundant power conversion • High efficiency	• The already available terminals are not used
D2A/A2D	• Eliminates one redundant power conversions • Four quadrant operation is possible • Medium efficiency	• The already available terminals are not used • One redundant power conversion
A2B/B2A	• The already available terminals are used • Four quadrant operation is possible • Medium efficiency	• One redundant power conversion
Proposed	• The converter of only one EV is used • The already available terminals are used • Eliminates two redundant power conversions • High Efficiency	• One redundant power conversion

4.9. Conclusion

A novel V2V charge transfer technique using the proposed bridgeless single-phase Cuk-derived converter with reduced components' count for the on-board EV charging application is

presented. A review of various V2V charge transfer technique has been discussed. The detailed steady-state analysis over one switching cycle is presented along with the design expressions derivation of the proposed converter in DC charging mode. The validity of the proposed power converter in DC charging mode for V2V power transfer is proved using the PSIM 11 simulation results. A 500 W rated proof-of-concept hardware prototype has been implemented to confirm the converter analysis and design. High efficiency of 95% is achieved from the laboratory hardware setup for the V2V power transfer. The losses occurring in different components of the power converter has been demonstrated along with the loss analysis. The achieved efficiency has been compared with several state-of-art V2V charge transfer techniques. Further, a comparative analysis of different configurations for V2V charging with the proposed configuration has been presented.

CHAPTER 5: CONCLUSIONS AND FUTURE WORK

EV adoption is a feasible solution to curb burning environment issues of greenhouse gas emission and global warming. Plug-in battery chargers are an essential part of the EV system. Development of high performance, highly efficient, cost-effective, light weight, reliable and compact battery chargers are fundamental to the success of the EVs in the consumer market. Improvement of EV charger input current power quality necessitates a PFC AC/DC converter. Further, to mitigate the range anxiety battery chargers incorporating flexible charging options such as V2V power transfer becomes meritorious. In order to reduce the size of the passive components, high frequency operation of the power converter is crucial. Usually, these EV chargers are separate for AC and DC charging so, they are unable to incorporate the option of flexible charging. This thesis puts forward a single-phase bridgeless Cuk-derived universal battery charger for G2V and V2V battery charging operations.

This Chapter puts forward the research and thesis contributions in Section 5.1. The future extension of this research work and findings are discussed in Section 5.2.

5.1. Thesis Contributions

This thesis contributes to the analysis and design of single-phase Cuk-derived PFC bridgeless power converter with primary goals of flexible battery charging, components reduction, power quality, and efficiency improvement. The converter is designed to operate in DCM to accomplish PFC naturally at the AC mains. The converter achieves high power factor along with THD (<5%) as per the standards. The DCM design also aids in simplifying the control circuit along with sensor reduction making the converter reliable and robust to high frequency noise. The main features of the Cuk-derived battery charger topology are improved efficiency, high power quality, simple control, and flexible charging. The contributions are highlighted as follows:

5.1.1. Single Sensor based Cuk Derived PFC Converter for G2V Charging

The first contribution of the thesis in Chapter 3 is the single phase bridgeless Cuk-derived PFC converter for G2V battery charging application. The key features of the power converter are the simple control, high power quality, improved efficiency, reduced components, and high density. The proposed converter has lower conduction losses as only semiconductor device is in

the current flow path throughout the converter operation thus, making the thermal management simpler. Also, the voltage stress is lower compared to the conventional Cuk converter, which reduces the switching losses. As a result, the overall system efficiency increases. The DCM design aids in accomplishing PFC naturally on the input side thereby, only a single voltage control loop and single voltage sensor are required for the control circuit making the circuit simpler. Detailed small signal modeling and controller design is presented. The topology has been compared to state-of-the art battery charging topologies to prove its competitive performance. A proof-of-concept laboratory prototype has been built and tested to validate the analysis, design, and performance of the power converter. The prototype is tested for the load perturbation as well as 25% source voltage disturbance. UPF is maintained in all the cases. Extensive loss analysis has been reported. The hardware prototype attains an efficiency of 94% with a power factor and THD of 0.9994 and 3.49%, respectively.

5.1.2. Single Phase Bridgeless Cuk Derived DC-DC Converter for V2V Charging

The second contribution of the thesis presented in Chapter 4 is the operation and analysis of the same converter topology for the V2V battery charging application (DC-DC operation). A novel V2V charge transfer technique has been implemented with the same topology to mitigate the range anxiety and enable flexible battery charging options for EV consumers in case of emergency. The reduced component count makes the on-board charger lightweight as well as the lower voltage stress decrease the switching losses and boosts the system efficiency. The proposed V2V charge transfer technique has been compared with several charge transfer technique reported in literature. The laboratory prototype has been tested to validate its V2V charging operation (DC-to-DC). Efficiency analysis has been conducted and a high efficiency of 95% has been achieved in the proof-of-concept hardware prototype.

In addition to the above contributions, the conclusions common to both the battery charger configuration are listed below:

- The converter is designed in DCM mode to reduce the complexity of control circuit.
- The steady-state analysis and design for both the configurations have been reported.

- The turn-on losses of the switches are zero and the diodes have zero reverse recovery losses, which are the characteristics of DCM design.
- The current rating of the semiconductor devices is high owing to the high current stress due to the DCM operation.
- Stiff 400V DC output has been attained.
- Simulation and experimental results are provided to validate the AC-DC and DC-DC operation of the topology and its performance.
- Efficiency above 94% is achieved in the laboratory developed prototype for both the configurations.

5.2. Future Scope of Research

The future research recommendations based on the findings of this work are summarised in the subsections below.

5.2.1. Analysis for Bidirectional Operation of the Converter for V2G, V2H and V2V Charge Transfer

The present plug-in battery chargers available in the market are unidirectional chargers. But with the smart grid concept EVs can feed back energy into the grid. Also, EV batteries can supply to residential loads during a power outage or peak demand that is transferring power from vehicle-to-home (V2H). The EVs can become more consumer friendly when it attains the capability to transfer the surplus energy to another EV with no charging stations nearby in case of emergency. To accomplish these operations, a bidirectional EV charger is necessary. Therefore, the proposed Cuk-derived topology can be investigated for its bidirectional capabilities both in AC-DC and DC-DC mode.

5.2.2. Closed Loop Control of the Bidirectional Power Flow for V2G, V2H and V2V Charge Transfer

A robust controller design becomes very crucial to control the bi-directional power flow to deliver constant power to the load as well as to switch among various modes of operation such as G2V, V2G, V2V, and V2H. Therefore, the design of closed loop control for the bidirectional power flow can be another possible research scope.

5.2.3. Converter Operation in CCM

The converter configurations can be analysed in CCM and designing the controller accordingly can be a future scope of research. It will reduce the current stress and will require reduced current rated components.

5.2.4. Efficiency Optimization

The hardware prototype is a proof-of-concept experimental unit and is not optimized. It is developed using off the shelf PCB and components to validate the proposed concept. The efficiency can be further enhanced by optimizing the PCB design and the components selection. The switches have the highest losses and the conduction loss can be reduced by selecting the switches with low on-state resistance.

5.3. Conclusion

This Chapter presents the contribution of this thesis and the future scope based on the research and findings. The major research contributions along with discussions on extending the research work has been highlighted.

REFERENCES

[1] R. Kushwaha and B. Singh, "Interleaved Landsman Converter Fed EV Battery Charger with Power Factor Correction," 2018 IEEE 8th Power India International Conference (PIICON), 2018, pp. 1-6, doi: 10.1109/POWERI.2018.8704418.

[2] "At what point is your EV truly more sustainable than a fossil fuel car?," *Allego*, 24-Oct-2019.[Online].Available: https://www.allego.eu/blog/2019/october/circular-thinking--carbon-footprint. [Accessed: 21-Jul-2021].

[3] R. Graham, "Hydrogen fuel cell vs electric cars: what you need to know," *euronews*,14-Feb-2020.[Online].Available: https://www.euronews.com/green/2020/02/13/hydrogen-fuel-cell-vs-electric-cars-what-you-need-to-know-but-couldn-t-ask. [Accessed: 21-Jul-2021].

[4] C. C. Chan, "The State of the Art of Electric, Hybrid, and Fuel Cell Vehicles," in Proceedings of the IEEE, vol. 95, no. 4, pp. 704-718, April 2007, doi: 10.1109/JPROC.2007.892489.

[5] M. S. Alam, T. Moeller and A. Maly, "Conversion of an Indian Three Wheeler Scooter into Hybrid Fuel Cell Ni-MH Battery Vehicle and Validation of the Vehicle Model for the Bajaj Three Wheeler Scooter," *2006 IEEE Conference on Electric and Hybrid Vehicles*, 2006, pp. 1-6, doi: 10.1109/ICEHV.2006.352283

[6] "Outlook for Electric Vehicles and Implications for the Oil Market" [Online]. Available:https://www.bankofcanada.ca/wp-content/uploads/2019/06/san2019 19.pdf

[7] "Electric Mobility: Taking the Pulse in Times of Coronavirus" [Online]. https://www.itf-oecd.org/sites/default/files/electric-vehicles-covid-19.pdf

[8] "Global BEV & PHEV Sales for 2019" [Online]. Available: https://www.evvolumes.com/

[9] S. Gangavarapu, A. K. Rathore, S. K. Mishra and R. K. Singh, "Analysis and Design of a Single-Phase Bridgeless Cuk-based PFC Converter as On-Board Charger with Reduced Number of Components and Losses," 2019 IEEE Transportation Electrification Conference (ITEC-India), 2019, pp. 1-6, doi: 10.1109/ITEC-India48457.2019.ITECINDIA2019-194.

[10] *Limits for Harmonic Current Emissions (Equipment Input Current <16A Per Phase)*, IEC/EN61000-3-2, 1995.

[11] K. Pande, "*Single-Sensor DCM PFC Based Onboard Chargers for Low Voltage Electric Vehicles,"* M.A.Sc. thesis, ECE., Concordia Univ., Montreal, QC, 2020.

[12] J. Xiaoping, "A new AC charging system with orderly charging for electric vehicles," 2013 5th International Conference on Power Electronics Systems and Applications(PESA), 2013, pp. 1-4, doi: 10.1109/PESA.2013.6828230.

[13] Bhatti, A. R., Salam, Z., Aziz, M. J. B. A., and Yee, K. P. (2016) A critical review of electric vehicle charging using solar photovoltaic. *Int. J. Energy Res.*, 40: 439– 461. doi: 10.1002/er.3472.

[14] P. Paulraj, "CHARGING BASICS 102: Electric Vehicle Charging Levels, Modes and Types Explained: North America Vs. Europe Charging cables and plug types," *E*. [Online]. Available: https://www.emobilitysimplified.com/2019/10/ev-charging-levels-modes-types-explained.html. [Accessed: 21-Jul-2021].

[15] A. Dixit, "*Analysis and Design of High Efficiency Grid-to-Vehicle (G2V) Plug-in Chargers for Local e-Transportation,"* M.A.Sc. thesis, ECE., Concordia Univ., Montreal, QC, 2020.

[16] J. Afsharian, D. Xu, T. Zhao, B. Gong and Z. Yang, "Reduced duty-cycle loss and output inductor current ripple in a ZVS switched three-phase isolated PWM rectifier," 2016 IEEE Applied Power Electronics Conference and Exposition (APEC), Long Beach, CA, 2016, pp. 33-37, doi: 10.1109/APEC.2016.7467848.

[17] C. Oh, D. Kim, D. Woo, W. Sung, Y. Kim and B. Lee, "A High-Efficient Non isolated Single-Stage On-Board Battery Charger for Electric Vehicles," in IEEE Transactions 83 on Power Electronics, vol. 28, no. 12, pp. 5746-5757, Dec. 2013, doi: 10.1109/TPEL.2013.2252200.

[18] R. Kushwaha and B. Singh, "UPF-isolated zeta converter-based battery charger for electric vehicle," in IET Electrical Systems in Transportation, vol. 9, no. 3, pp. 103-112, 9 2019, doi: 10.1049/iet-est.2018.5010.

[19] J. Lee and H. Chae, "6.6-kW Onboard Charger Design Using DCM PFC Converter With Harmonic Modulation Technique and Two-Stage DC/DC Converter," in IEEE Transactions on Industrial Electronics, vol. 61, no. 3, pp. 1243-1252, March 2014, doi: 10.1109/TIE.2013.2262749.

[20] R. Kushwaha and B. Singh, "A Modified Luo Converter-Based Electric Vehicle Battery Charger With Power Quality Improvement," in IEEE Transactions on Transportation Electrification, vol. 5, no. 4, pp. 1087-1096, Dec. 2019, doi: 10.1109/TTE.2019.2952089.

[21] Rapidtron Electronika Private Limited ” [online]: Available: http://rapidtron.co.in/3- wheeler-chargers/

[22] S. Gangavarapu, A. K. Rathore and D. M. Fulwani, "Three-Phase Single-StageIsolated Cuk-Based PFC Converter," in IEEE Transactions on Power Electronics, vol. 34, no. 2, pp. 1798-1808, Feb. 2019, doi: 10.1109/TPEL.2018.2829080

[23] Rapidtron Electronika Private Limited ” [online]: Available: “http://rapidtron.co.in/3- wheeler-chargers/

[24] R. Kushwaha and B. Singh, "A Bridgeless Isolated Half Bridge Converter Based EV Charger with Power Factor Pre-regulation," 2019 IEEE Transportation Electrification Conference (ITEC-India), 2019, pp. 1-6, doi: 10.1109/ITEC-India48457.2019.ITECINDIA2019-190.

[25] J. Lee, Y. Jeong and B. Han, "An Isolated DC/DC Converter Using High-Frequency Unregulated LLC Resonant Converter for Fuel Cell Applications," in IEEE Transactions on Industrial Electronics, vol. 58, no. 7, pp. 2926-2934, July 2011, doi: 10.1109/TIE.2010.2076311.

[26] K. Yoo, K. Kim and J. Lee, "Single- and Three-Phase PHEV Onboard Battery Charger Using Small Link Capacitor," in IEEE Transactions on Industrial Electronics, vol. 60, no. 8, pp. 3136-3144, Aug. 2013, doi: 10.1109/TIE.2012.2202361.

[27] D. S. Gautam, F. Musavi, M. Edington, W. Eberle and W. G. Dunford, "An Automotive Onboard 3.3-kW Battery Charger for PHEV Application," in IEEE Transactions on Vehicular Technology, vol. 61, no. 8, pp. 3466-3474, Oct. 2012, doi: 10.1109/TVT.2012.2210259.

[28] H. Wang, S. Dusmez and A. Khaligh, "Design and Analysis of a Full-Bridge LLC-Based PEV Charger Optimized for Wide Battery Voltage Range," in IEEE Transactions on Vehicular Technology, vol. 63, no. 4, pp. 1603-1613, May 2014, doi: 10.1109/TVT.2013.2288772.

[29] F. Musavi, M. Craciun, D. S. Gautam, W. Eberle and W. G. Dunford, "An LLC Resonant DC–DC Converter for Wide Output Voltage Range Battery Charging Applications," in IEEE Transactions on Power Electronics, vol. 28, no. 12, pp. 5437-5445, Dec. 2013, doi: 10.1109/TPEL.2013.2241792.

[30] H. J. Chae, W. Y. Kim, S. Y. Yun, Y. S. Jeong, J. Y. Lee and H. T. Moon, "3.3kW on board charger for electric vehicle," 8th International Conference on Power

Electronics - ECCE Asia, Jeju, 2011, pp. 2717-2719, doi: 10.1109/ICPE.2011.5944762.

[31] F. Musavi, W. Eberle and W. G. Dunford, "A High-Performance Single-Phase Bridgeless Interleaved PFC Converter for Plug-in Hybrid Electric Vehicle Battery Chargers," in IEEE Transactions on Industry Applications, vol. 47, no. 4, pp. 1833-1843, July-Aug. 2011, doi: 10.1109/TIA.2011.2156753.

[32] Gwan-Bon Koo, Gun-Woo Moon and Myung-Joong Youn, "New zero-voltageswitching phase-shift full-bridge converter with low conduction losses," in IEEE Transactions on Industrial Electronics, vol. 52, no. 1, pp. 228-235, Feb. 2005, doi: 10.1109/TIE.2004.841063.

[33] M. Brunoro and J. L. F. Vieira, "A high-performance ZVS full-bridge DC-DC 0-50- V/0-10-A power supply with phase-shift control," in IEEE Transactions on Power Electronics, vol. 14, no. 3, pp. 495-505, May 1999, doi: 10.1109/63.761693.

[34] S. Moisseev, S. Hamada and M. Nakaoka, "Full-bridge soft-switching phase-shifted PWM DC-DC power converter using tapped inductor filter," in Electronics Letters, vol. 39, no. 12, pp. 924-925, 12 June 2003, doi: 10.1049/el:20030604.

[35] Song-Yi Lin and Chern-Lin Chen, "Analysis and design for RCD clamped snubber used in output rectifier of phase-shift full-bridge ZVS converters," in IEEE Transactions on Industrial Electronics, vol. 45, no. 2, pp. 358-359, April 1998, doi: 10.1109/41.681236.

[36] Y. Wei, Q. Luo and A. Mantooth, "Comprehensive analysis and design of LLC resonant converter with magnetic control," in CPSS Transactions on Power Electronics and Applications, vol. 4, no. 4, pp. 265-275, Dec. 2019, doi: 10.24295/CPSSTPEA.2019.00025.

[37] M. F. Menke, Á. R. Seidel and R. V. Tambara, "LLC LED Driver Small-Signal Modeling and Digital Control Design for Active Ripple Compensation," in IEEE Transactions on Industrial Electronics, vol. 66, no. 1, pp. 387-396, Jan. 2019, doi: 10.1109/TIE.2018.2829683.

[38] M. Mohammadi, F. Degioanni, M. Mahdavi and M. Ordonez, "Small-Signal Modeling of LLC Converters Using Homopolarity Cycle," in IEEE Transactions on Power Electronics, vol. 35, no. 4, pp. 4076-4093, April 2020, doi: 10.1109/TPEL.2019.2933179.85

[39] S. Shah, P. Koralewicz, V. Gevorgian and L. Parsa, "Small-Signal Modeling and Design of Phase-Locked Loops Using Harmonic Signal-Flow Graphs," in IEEE

Transactions on Energy Conversion, vol. 35, no. 2, pp. 600-610, June 2020, doi: 10.1109/TEC.2019.2954112.

[40] A. V. J. S. Praneeth, D. Vincent and S. S. Williamson, "An Universal On-board Battery Charger with Wide Output Voltage Range for Electric Transportation," 2019 IEEE Energy Conversion Congress and Exposition (ECCE), Baltimore, MD, USA, 2019, pp. 1159-1165, doi: 10.1109/ECCE.2019.8912749.

[41] T. Bohn and H. Chaudhry, "Overview of SAE standards for plug-in electric vehicle," 2012 IEEE PES Innovative Smart Grid Technologies (ISGT), Washington, DC, 2012, pp. 1-7, doi: 10.1109/ISGT.2012.6175597.

[42] M. Yilmaz and P. T. Krein, "Review of Battery Charger Topologies, Charging Power Levels, and Infrastructure for Plug-In Electric and Hybrid Vehicles," in *IEEE Transactions on Power Electronics*, vol. 28, no. 5, pp. 2151-2169, May 2013, doi: 10.1109/TPEL.2012.2212917.

[43] H. Li, S. Wang, Z. Zhang, J. Tang, X. Ren and Q. Chen, "A SiC Bidirectional LLC On-Board Charger*," 2019 IEEE Applied Power Electronics Conference and Exposition (APEC), Anaheim, CA, USA, 2019, pp. 3353-3360.

[44] H. V. Nguyen and D. Lee, "Advanced Single-Phase Onboard Chargers with Small DC-Link Capacitors," 2018 IEEE International Power Electronics and Application Conference and Exposition (PEAC), Shenzhen, 2018, pp. 1-6.

[45] S. Bolte, A. Speerschneider, N. Fröhleke and J. Böcker, "A comparison of on-board chargers for electric vehicles with variable DC-link voltage," 2015 IEEE International Conference on Smart Energy Grid Engineering (SEGE), Oshawa, ON, 2015, pp. 1-5.

[46] R. Kushwaha and B. Singh, "A Power Quality Improved EV Charger with Bridgeless Cuk Converter," in IEEE Transactions on Industry Applications, 2019.

[47] M. Nassary, M. Orabi and M. Ghoneima, "Discussion of Single-Stage Isolated Unidirectional AC-DC On-Board Battery Charger for Electric Vehicle," 2018 IEEE 4th Southern Power Electronics Conference (SPEC), Singapore, Singapore, 2018, pp. 1-7.

[48] B. Kim, M. Kim and S. Choi, "A reduced component count single-stage electrolytic capacitor-less battery charger with sinusoidal charging," 2017 IEEE 3rd International Future Energy Electronics Conference and ECCE Asia (IFEEC 2017 - ECCE Asia), Kaohsiung, 2017, pp. 242-246.

[49] D. Patil, M. Sinha and V. Agarwal, "A cuk converter based bridgeless topology for high power factor fast battery charger for Electric Vechicle application," 2012 IEEE Transportation Electrification Conference and Expo (ITEC), Dearborn, MI, 2012, pp. 1-6.

[50] B. Singh and R. Kushwaha, "An EV battery charger with power factor corrected bridgeless zeta converter topology," 2016 7th India International Conference on Power Electronics (IICPE), Patiala, 2016, pp. 1-6.

[51] B. Singh and R. Kushwaha, "A PFC based EV battery charger using a bridgeless SEPIC converter," 2016 IEEE 7th Power India International Conference (PIICON), Bikaner, 2016, pp. 1-6

[52] P. Y. Kong, J. A. Aziz, M. R. Sahid and L. W. Yao, "A bridgeless PFC converter for on-board battery charger," 2014 IEEE Conference on Energy Conversion (CENCON), Johor Bahru, 2014, pp. 383-388.

[53] A. A. Fardoun, E. H. Ismail, A. J. Sabzali, and M. A. Al-Saffar, "New efficient bridgeless Cuk rectifiers for PFC applications," IEEE Trans. Power Electron., vol. 27, no. 7, pp. 3292–3301, Jul. 2012.

[54] M. R. Sahid, A. H. M. Yatim, and N. D. Muhammad, "A bridgeless Cuk PFC converter," in Proc. IEEE Appl. Power Electron. Colloq., 2011, pp. 81–85.

[55] M. Mahdavi and H. Farzaneh-Fard, "Bridgeless CUK power factor correction rectifier with reduced conduction losses," IET Power Electron., vol. 5, no. 9, pp. 1733–1740, Nov. 2012.

[56] P. R. K. Chetty, "Current Injected Equivalent Circuit Approach to Modeling of Switching DC-DC Converters in Discontinuous Inductor Conduction Mode," in *IEEE Transactions on Industrial Electronics*, vol. IE-29, no. 3, pp. 230-234, Aug. 1982, doi: 10.1109/TIE.1982.356670.

[57] R. Kushwaha and B. Singh, "An improved battery charger for electric vehicle with high power factor," in Proc. IEEE Ind. Appl. Soc. Annu. Meet.,2018,pp.1–8.

[58] A. J. Sabzali, E. H. Ismail, M. A. Al-Saffar, and A. A. Fardoun, "New bridgeless DCM sepic and Cuk PFC rectifiers with low conduction and switching losses," IEEE Trans. Ind. Appl., vol. 47, no. 2, pp. 873–881, Mar./Apr. 2011.

[59] R. Kushwaha, B. Singh and V. Khadkikar, "An Improved PQ Zeta Converter with Reduced Switch Voltage Stress for Electric Vehicle Battery Charger," *2020 IEEE Energy Conversion Congress and Exposition (ECCE)*, 2020, pp. 858-863, doi: 10.1109/ECCE44975.2020.923611

[60] "An Efficiency Primer for Switch-Mode, DC-: Maxim Integrated," *An Efficiency Primer for Switch-Mode, DC- | Maxim Integrated*. [Online]. Available: https://www.maximintegrated.com/en/design/technical-documents/app-notes/4/4266.html.

[61] A. K. Singh, E. Jeyasankar, P. Das and S. K. Panda, "A Matrix-Based Nonisolated Three-Phase AC-DC Rectifier With Large Step-Down Voltage Gain," in *IEEE Transactions on Power Electronics,* vol. 32, no. 6, pp.4796-4811, June 2017.

[62] E. Bulut and M. C. Kisacikoglu, "Mitigating Range Anxiety via Vehicle-to-Vehicle Social Charging System," 2017 IEEE 85th Vehicular Technology Conference (VTC Spring), 2017, pp. 1-5, doi: 10.1109/VTCSpring.2017.8108288.

[63] I. N. L. (INL), "Plugged in: How americans charge their electric vehicles," 2015. [Online]. Available: http://avt.inel.gov/pdf/ arra/SummaryReport.pdf

[64] M. Nasr, K. Gupta, C. da Silva, C. H. Amon, and O. Trescases, "SiC based onboard EV power-hub with high-efficiency DC transfer mode through AC port for vehicle-to-vehicle charging," in 2018 IEEE Applied Power Electronics Conference and Exposition (APEC), 2018, vol. 1, pp. 3398–3404.

[65] W. Kempton and J. Tomić, "Vehicle-to-grid power implementation: From stabilizing the grid to supporting large-scale renewable energy," Journal of Power Sources, vol. 144, no. 1, pp. 280–294, 2005.

[66] G. Haines and A. McGordon, "The simulation of vehicle-to-home systems - Using electric vehicle battery storage to smooth domestic electricity demand," Proceedings Ecologic Vehicles/Renewable Energies - EVRE, Dec., pp. 1–9, 2009.

[67] D. P. Tuttle and R. Baldick, "The evolution of plug-in electric vehicle-grid interactions," IEEE Transactions on Smart Grid, vol. 3, no. 1, pp. 500–505, 2012.

[68] M. Brenna, F. Foiadelli, and M. Longo, "The exploitation of vehicle-to-grid function for power quality improvement in a smart grid," IEEE Transactions on Intelligent Transportation Systems, vol. 15, no. 5, pp. 2169–2177, 2014.

[69] M. Kesler, M. C. Kisacikoglu, and L. M. Tolbert, "Vehicle-to-Grid Reactive Power Operation Using Plug-In Electric Vehicle Bidirectional Offboard Charger," IEEE Transactions on Industrial Electronics, vol. 61, no. 12, pp. 6778–6784, 2014.

[70] N. Z. Xu, C. Y. Chung, and S. Member, "Reliability Evaluation of Distribution Systems Including Vehicle-to-Home and Vehicle-to-Grid," IEEE Transactions on Power Systems, pp. 1–10, 2015.

[71] V. Monteiro, J. G. Pinto, and J. L. Afonso, “Operation Modes for the Electric Vehicle in Smart Grids and Smart Homes: Present and Proposed Modes,” IEEE Transactions on Vehicular Technology, vol. 65, no. 3, pp. 1007–1020. 2016

[72] T. J. C. Sousa, L. Machado, D. Pedrosa, C. Martins, V. Monteiro and J. L. Afonso, "Comparative Analysis of Vehicle-to-Vehicle (V2V) Power Transfer Configurations without Additional Power Converters," 2020 IEEE 14th International Conference on Compatibility, Power Electronics and Power Engineering (CPE-POWERENG), 2020, pp. 88-93, doi: 10.1109/CPE-POWERENG48600.2020.9161697.

[73] T. J. C. Sousa, V. Monteiro, J. C. A. Fernandes, C. Couto, A. A. N. Meléndez and J. L. Afonso, "New Perspectives for Vehicle-to-Vehicle (V2V) Power Transfer," IECON 2018 - 44th Annual Conference of the IEEE Industrial Electronics Society, 2018, pp. 5183-5188, doi: 10.1109/IECON.2018.8591209.

[74] C. Liu, K. T. Chau, D. Wu, and S. Gao, “Opportunities and challenges of vehicle-to-home, vehicle-to-vehicle, and vehicle-to-grid technologies,” Proceedings of the IEEE, vol. 101, no. 11, pp. 2409–2427, 2013.

[75] R. Alvaro, J. Gonzalez, C. Gamallo, J. Fraile-Ardanuy, and L. Knapen, “Vehicle to vehicle energy exchange in smart grid applications,” IEEE Conference on Connected Vehicles and Expo, pp. 1–7, 2014.

[76] P. You and Z. Yang, “Efficient optimal scheduling of charging station with multiple electric vehicles via V2V,” in 2014 IEEE International Conference on Smart Grid Communications (SmartGridComm), 2014, pp. 716–721.

[77] R. Alvaro-Hermana, J. Fraile-Ardanuy, P. J. Zufiria, L. Knapen, and D. Janssens, “Peer to Peer Energy Trading with Electric Vehicles,” IEEE Intelligent Transportation Systems Magazine, vol. 8, no. 3, pp. 33–44, 2016.

[78] M. A. Masrur et al., “Military-Based Vehicle-to-Grid and Vehicle-to-Vehicle Microgrid—System Architecture and Implementation,” IEEE Transactions on Transportation Electrification, vol. 4, no. 1, pp.157–171, 2018.

[79] C. Samende, N. Mugwisi, D. J. Rogers, E. Chatzinikolaou, F. Gao and M. McCulloch, "Power Loss Analysis of a Multiport DC – DC Converter for DC Grid Applications," IECON 2018 - 44th Annual Conference of the IEEE Industrial Electronics Society, 2018, pp. 1412-1417, doi: 10.1109/IECON.2018.8591730.

[80] S. Tandon, A. K. Rathore and J. Rodriguez, "Partial Series Resonance Pulse Commutated Current-Fed Three-phase current sharing DC/DC Converter: ZCS Analysis, Design and Experimental Results," in IEEE Journal of Emerging and Selected Topics in Industrial Electronics, doi: 10.1109/JESTIE.2021.3074876.

[81] D. Lyu, T. B. Soeiro and P. Bauer, "Impacts of Different Charging Strategies on the Electric Vehicle Battery Charger Circuit Using Phase-Shift Full-Bridge Converter," 2021 IEEE 19th International Power Electronics and Motion Control Conference (PEMC), 2021, pp. 256-263, doi: 10.1109/PEMC48073.2021.9432497.

[82] Marketing, “What to know about electric vehicles in hot weather,” EVSolutions Blog. [Online]. Available: https://blog.evsolutions.com/electric-vehicles-in-hot-weather.

[83] “How temperature affects ev range,” Recurrent. [Online]. Available: https://www.recurrentauto.com/research/how-temperature-affects-ev-range.

PUBLICATIONS

Journal Proceedings

1. **S. Dutta**, S. Gangavarapu, A. K. Rathore, R. K. Singh, S. K. Mishra, V. Khadkikar "Novel Single-Phase Bridgeless Cuk-derived PFC Converter for On-Board EV Charger with Reduced Number of Components," in *IEEE Transactions on Industry Applications*. **(1st Revision/Under Review)**

Conference Proceedings

1. **S. Dutta**, S. Gangavarapu, V. R. Vakacharla, A. K. Rathore "Small Signal Analysis and Control of Single-Phase Briddgeless Cuk-based PFC Converter for On-Board EV Charger," *2021 IEEE Transportation Electrification Conference (ITEC-USA),* Chicago, USA, 2021. **(Accepted)**

2. **S. Dutta**, A. K. Rathore "Analysis and Design of Single-Phase Bridgeless Cuk-derived DC-DC Converter for Vehicle-to-Vehicle Charge Transfer as On-Board EV Charger," *IECON 2021 The 47th Annual Conference of the IEEE Industrial Electronics Society,* 2021. **(Submitted)**